

# Master Thesis

# Morphology Optimization of a Tilt-Rotor MAV

Spring Term 2018



## Declaration of Originality

I hereby declare that the written work I have submitted entitled  
**Morphology Optimization of a Tilt-Rotor MAV**  
is original work which I alone have authored and which is written in my own words.<sup>1</sup>

### Author(s)

Luca Rinsoz

### Student supervisor(s)

Karen Bodie  
Zachary Taylor

### Supervising lecturer

Roland Siegwart

With the signature I declare that I have been informed regarding normal academic citation rules and that I have read and understood the information on 'Citation etiquette' (<https://www.ethz.ch/content/dam/ethz/main/education/rechtliches-abschluesse/leistungskontrollen/plagiarism-citationetiquette.pdf>). The citation conventions usual to the discipline in question here have been respected.

The above written work may be tested electronically for plagiarism.

Zürich, 10<sup>th</sup> September 2018

Place and date



Signature

<sup>1</sup>Co-authored work: The signatures of all authors are required. Each signature attests to the originality of the entire piece of written work in its final form.

# Contents

<b>Abstract</b>	<b>iii</b>
<b>Symbols</b>	<b>v</b>
<b>1 Introduction</b>	<b>1</b>
<b>2 Method</b>	<b>3</b>
2.1 Modelisation of MAVs . . . . .	4
2.2 Optimization problem . . . . .	6
2.3 Optimization tool . . . . .	8
2.4 Simulation Approach . . . . .	10
<b>3 Optimization Results</b>	<b>11</b>
3.1 Platonic Solids . . . . .	11
3.2 Even Designs . . . . .	12
3.2.1 Quad-copter . . . . .	12
3.2.2 Hexa-copter . . . . .	15
3.2.3 Octa-copter . . . . .	17
3.3 Odd Designs . . . . .	20
3.3.1 Penta-copter . . . . .	20
3.3.2 Hepta-copter . . . . .	22
3.4 Comparison of Different Designs . . . . .	23
<b>4 Simulation Results</b>	<b>27</b>
4.1 Tri-copter . . . . .	27
4.2 Hexa-copter . . . . .	28
4.3 Hepta-copter . . . . .	33
<b>5 Conclusion</b>	<b>35</b>
<b>Bibliography</b>	<b>37</b>
<b>Acknowledgements</b>	<b>39</b>

# Abstract

Selecting an optimal morphology of an omni-directional flying platform with changing propeller axes is not a straightforward problem. Various factors influence the desired morphology, such as flight efficiency, omni-directionality, and control authority. In the present work the development of a tool that solves the design optimization problem for a tilt-rotor MAV is presented. Different optimal morphologies are then acquired. Finally, a verification of the proposed platforms is completed in different simulations.



# Symbols

## Symbols

$\phi, \theta, \psi$	roll, pitch and yaw angle
$\beta_{PS}$	platonic solid angle
$\beta_{arm,i}$	angle between horizontal plan and MAV's i-th arm
$\theta_{arm,i}$	angle formed by the MAV's i-th arm in the horizontal plan
$\mathcal{F}_W$	inertial world frame
$\mathcal{F}_B$	inertial body frame
$\mathcal{F}_{P_i}$	i-th propeller frame
$p$	position of the MAV in $\mathcal{F}_W$
$\omega_B$	angular velocity of the MAV in $\mathcal{F}_B$
${}^W R_B$	rotation matrix from $\mathcal{F}_B$ to $\mathcal{F}_W$
${}^B R_{P_i}$	rotation matrix from $\mathcal{F}_{P_i}$ to $\mathcal{F}_B$
$R_X(\gamma)$	canonical rotation matrix about the $X$ axis of angle $\gamma$
$R_Y(\gamma)$	canonical rotation matrix about the $Y$ axis of angle $\gamma$
$R_Z(\gamma)$	canonical rotation matrix about the $Z$ axis of angle $\gamma$
$\alpha_i$	i-th propeller tilt angle
$w_i$	i-th propeller rotation speed
$\tau_{ext_i}$	i-th propeller counter rotation torque
$T_i$	i-th thrust
$m$	total mass of the MAV
$I_B$	body inertia of the MAV
$n$	MAV's number of propellers
$L$	MAV's arms length
$\kappa_f$	propeller thrust coefficient
$\kappa_m$	propeller drag coefficient
$g$	gravity constant
$c(\gamma)$	cosine of the angle $\gamma$
$s(\gamma)$	sine of the angle $\gamma$

## Acronyms and Abbreviations

ccw	counterclockwise
cw	clockwise
CoM	Center of Mass

DoF	Degrees of Freedom
ETH	Eidgenössische Technische Hochschule
GUI	Graphical User Interface
MAD	Mean Absolute Deviation
MAV	Micro Aerial Vehicle
ROS	Robotic Operating System
sqp	sequential quadratic programming
UAV	Unmanned Aerial Vehicle
URDF	Unified Robot Description Format

# Chapter 1

## Introduction

Rotary wing micro aerial vehicles (MAVs) have been well studied in academia and found a lot of applications in the world such as search operations [1], photography [2] or even toys [3]. They encountered such a broad success because of their agility and mechanical simplicity. Nevertheless, traditional multi-rotor vehicles are under-actuated, which means that they cannot control their torque and force independently [4]. They are thus unable to change their position without changing their orientation.

Recently the focus has been on designing MAVs able to perform more complex tasks such as camera motion for the film industry [5] or bridge inspection where huge resources (i.e. cranes and large man-power) are needed. The ultimate goal would be for a drone to be able to interact with its surrounding and apply forces to it, in order to perform maintenance where humans can not access, or to do construction work in harsh environments.

To perform these tasks, an MAV has to be able to hover in any orientation, and for a proper disturbance rejection while manipulating, the drone must have the potential to accelerate instantaneously in any direction. Hence, the MAV has to be able to decouple its orientation and position control. A drone that has a decoupled force and torque control is referred to as an omni-directional MAV.

The problem of overcoming the under-actuation and achieving omni-directionality is not straightforward. To address this problem, several MAV designs have been presented over the past years. For instance, in [5], Voliro (name of the vehicle) is based on a traditional hexa-copter (see Figure 1.1). The omni-directionality issue is addressed by adding motors to rotate the thrusters around their arm axis, thus allowing a control not only of the thrust produced by each propeller, but also of the orientation of this thrust. This tilting rotor system allows for decoupling the control of position and orientation. By using a control scheme based on an allocation technique, the system provides very good maneuverability.



Figure 1.1: Voliro [5].

In [4], the Omnicopter (name of the vehicle) is described. It is a drone with eight fixed rotors and the drone shape is the result of a mathematical optimization which maximizes the vehicle's agility with the constraint that its dynamical properties would be as independent as possible on the vehicle's orientation (see Figure 1.2).

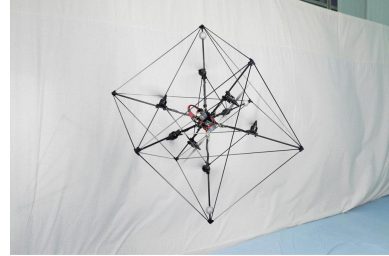


Figure 1.2: Omnicopter [4].

In [6], the MAV is a fixed propeller multi-rotor. The design is also the result of an optimization, which tends to minimize the body volume, to maximize the controllability of the system, avoid eventual aerodynamic interactions and to maximizes the efficiency in performing manipulation tasks.

The idea presented in [7] is a mix between Voliro and the Omnicopter because the design is a modified hexarotor, which achieves full control over the vehicle's position and orientation using manually tiltable propellers (see Figure 1.3). The paper also provides a methodology to optimize the fixed tilting angles depending on the desired trajectory.



Figure 1.3: Hexacopter with manually tilttable rotors [7].

Yet, nothing in the literature is found about the morphology optimization of MAVs with tilting rotors. Hence the need for the present research project. The aim of this thesis is thus to design a morphology optimization problem for a tilt-rotor MAV that accounts for the different factors that influence the morphology such as:

- Omni-directionality
- Flight efficiency
- Controlability

To reach this goal the chosen approach is to build an optimization tool that solves the optimization problem and returns different MAV designs. The most interesting designs are then tested in simulation. In this report the methods used to build the optimization tool and to simulate the results are discussed. Afterwards, the results returned by the tool are shown and compared based on different criteria. Finally, the results gathered during the simulation phase are also covered.

# Chapter 2

## Method

As explained in Chapter 1 the aim of this work is to find a drone design that is the result of an optimization problem, which tends to maximize the MAV's omnidirectionality, flight efficiency and controllability. In order to achieve this goal, it is, first of all, important to state which parameters will be used to define the design of an MAV. These parameters are defined as:

- $\beta_{arm}$  (angles formed by the arms with the horizontal plane see Figure 2.1)
- $\theta_{arm}$  (angles formed by the arms in the horizontal plane see Figure 2.1)
- $L$  (arm length)
- $n$  (number of propellers)

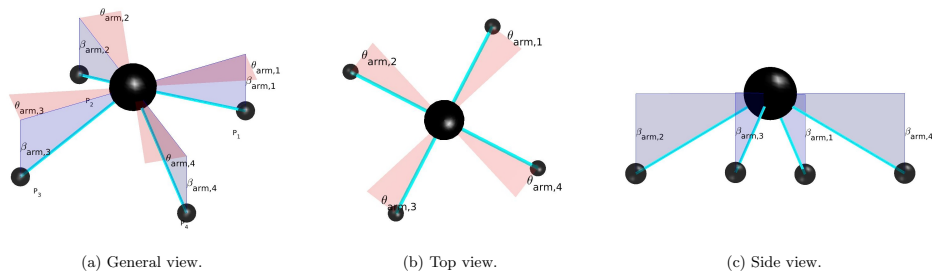


Figure 2.1: Arbitrary quad-copter design to illustrate the parameters that define the morphology of an MAV (with  $n = 4$ ,  $\beta_{arm} = [30^\circ, 30^\circ, 30^\circ, 30^\circ]$ ,  $\theta_{arm} = [22^\circ, 22^\circ, 22^\circ, 22^\circ]$ , and  $L = 0.4 [m]$ ).

To solve the problem, an optimization software or tool is developed with MATLAB<sup>®</sup><sup>1</sup>. This tool returns the aforementioned parameters along with other information on the corresponding MAV design. The interesting drone designs which result from the tool are then simulated on Gazebo<sup>®</sup><sup>2</sup> and the control of the different models is achieved using a Robotic Operating System<sup>3</sup> (ROS) node.

This chapter first covers the theory needed to obtain a generalized mathematical model for a n-rotor MAV with an arbitrary morphology. Then, the optimization problem is defined. Afterwards, the optimization tool is described. In the end, the theoretical background needed to perform the simulations is covered.

<sup>1</sup>A numerical computing environment and programming language developed by MathWorks<sup>®</sup> [8].

<sup>2</sup>An open source robot simulation software [9].

<sup>3</sup>An open source collection of software that help developers to create robot applications [10].

## 2.1 Modelisation of MAVs

In the following part, a dynamical model for a general design of an MAV is presented. Such a modelisation is needed to mathematically optimize the morphology of an MAV. This model is inspired by the models presented in [5] and [11].

### Assumptions

In this model, the first assumption is that the MAV is composed of  $n+1$  rigid bodies: one for each propeller unit  $P_i$  and one for the body  $B$ . Then, it is considered that the thrust is produced by irreversible fixed-pitch motor-propeller actuators. Finally, only the aerodynamic forces and torques that are responsible for the MAV actuation are considered, all the second order effects and disturbances are neglected as well as the airflow interactions between the rotors are neglected.

### Initial Definitions

In order to understand correctly the dynamical model, a few definitions are needed. First, let us define  $\mathcal{F}_W : \{O_W; X_W, Y_W, Z_W\}$  as the world fixed inertial frame and  $\mathcal{F}_B : \{O_B, X_B, Y_B, Z_B\}$  as a moving frame attached to the MAV. Also,  $\mathcal{F}_{P_i} : \{O_{P_i}; X_{P_i}, Y_{P_i}, Z_{P_i}\}, i = 1 \dots n$  is the frame of the  $i$ -th propeller. The propeller rotates around the axis  $Z_{P_i}$ , and thus the thrust  $T_i$  is produced along this axis. The tilt movement of the rotors is a simple rotation around  $X_{P_i}$ . Now let  ${}^W R_B$  be the orientation of the body frame with respect to the world frame and  ${}^B R_{P_i}$  be the orientation of the  $i$ -th propeller with respect to the body frame. It is straightforward with the help of Figure 2.2 that

$${}^B R_{P_i} = R_Z \left( (i-1) \frac{2\pi}{n} \right) R_Z(\theta_{arm,i}) R_Y(\beta_{arm,i}) R_X(\alpha_i), \quad i = 1 \dots n. \quad (2.1)$$

Equivalently, let

$${}^B O_{P_i} = R_Z \left( (i-1) \frac{2\pi}{n} \right) R_Z(\theta_{arm,i}) R_Y(\beta_{arm,i}) \begin{bmatrix} L \\ 0 \\ 0 \end{bmatrix}, \quad i = 1 \dots n \quad (2.2)$$

be the origin of the  $i$ -th propeller frame  $\mathcal{F}_{P_i}$ . In Equation (2.1) and (2.2),  $(i-1) \frac{2\pi}{n}$  is the angle that the  $i$ -th arm would form with axis  $X_B$  if the arms of the drone are evenly distributed in the horizontal plane,  $\theta_{arm,i}$  is the angle that  $i$ -th arm forms in the horizontal plane with respect to its evenly distributed position (see Figure 2.1),  $\beta_{arm,i}$  is the angle that the  $i$ -th arm forms with the horizontal plane (see Figure 2.1),  $\alpha_i$  is the tilting angle of the  $i$ -th propeller about the  $X_{P_i}$  axis,  $L$  is the arm length and  $n$  is the number of propellers.

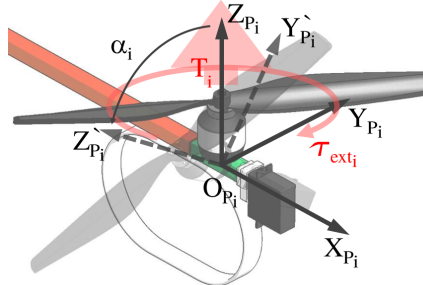


Figure 2.2: Representation of the  $i$ -th tilting arm [11].

### Equations of motion

Using Newton-Euler formalism, the general equations of motion of the MAV are

$$\begin{cases} \dot{\omega}_B = I_B^{-1} \sum_{i=1}^n ({}^B R_{P_i} \tau_{ext,i} + \tau_{Bi}) , \\ \ddot{p} = \begin{bmatrix} 0 \\ 0 \\ -g \end{bmatrix} \frac{1}{m} {}^W R_B \sum_{i=1}^n T_i . \end{cases} \quad (2.3)$$

Where

$$\tau_{Bi} = {}^B O_{P_i} \times {}^B R_{P_i} T_{P,i} , \quad (2.4)$$

$$\tau_{ext,i} = [0, 0, -c_i \kappa_m w_i^2]^T , \quad (2.5)$$

$$\begin{cases} c_i = 1, & \text{if } i \text{ is odd (cw rotation to produce + thrust)} \\ c_i = -1 & \text{if } i \text{ is even (ccw rotation to produce + thrust)} \end{cases}$$

and

$$T_i = {}^B R_{P_i} T_{P,i} , \quad T_{P,i} = [0, 0, \kappa_f w_i^2]^T . \quad (2.6)$$

In Equation (2.3)  $g$  is the gravity constant, in Equation (2.5)  $\kappa_m$  is the propeller drag coefficient, in Equation (2.6)  $\kappa_f$  is the propeller thrust coefficient and in Equations (2.5) and (2.6)  $w_i$  is the  $i$ -th propeller rotation speed. The force and torque that the drone produces in body frame  $\mathcal{F}_B$  are

$$\begin{bmatrix} M_B \\ F_B \end{bmatrix} = \left[ \sum_{i=1}^n ({}^B R_{P_i} \tau_{ext,i} + \tau_{Bi}) \right] , \quad (2.7)$$

that can be rewritten

$$\begin{bmatrix} M_B \\ F_B \end{bmatrix} = A(\alpha) W . \quad (2.8)$$

Where  $W = [w_1^2, w_2^2, \dots, w_n^2]$  and

$$A(\alpha) = \begin{bmatrix} (-\kappa_f L s(\beta_{arm,1}) c(\theta_{arm,1}) + c_1 \kappa_m s(\theta_{arm,1})) s(\alpha_1) + (\kappa_f L s(\theta_{arm,1}) + c_1 \kappa_m c(\theta_{arm,1}) s(\beta_{arm,1})) c(\alpha_1) & \dots \\ (-\kappa_f L s(\beta_{arm,1}) s(\theta_{arm,1}) - c_1 \kappa_m c(\theta_{arm,1}) s(\alpha_1) + (-\kappa_f L c(\theta_{arm,1}) + c_1 \kappa_m s(\beta_{arm,1}) s(\theta_{arm,1})) c(\alpha_1)) & \dots \\ (-L \kappa_f c(\beta_{arm,1})) s(\alpha_1) + (c_1 \kappa_m c(\beta_{arm,1})) c(\alpha_1) & \dots \\ s(\theta_{arm,1}) \kappa_f s(\alpha_1) + s(\beta_{arm,1}) c(\theta_{arm,1}) \kappa_f c(\alpha_1) & \dots \\ -c(\theta_{arm,1}) \kappa_f s(\alpha_1) + s(\beta_{arm,1}) s(\theta_{arm,1}) \kappa_f c(\alpha_1) & \dots \\ c(\beta_{arm,1}) \kappa_f c(\alpha_1) & \dots \end{bmatrix}$$

is the  $6 \times n$  allocation matrix and  $c(\cdot)$  and  $s(\cdot)$  represent the cosine and sine operator respectively.

### Static allocation

The optimization tool has to compute the maximal reachable force and torque in a large number of directions. So to compute that in a reasonable time in [5] an approach to transform the non-linear allocation matrix into a static allocation matrix, which renders the problem of inverse kinematic linear, is presented. To do so, the system in Equation (2.8) is rewritten as

$$\begin{bmatrix} M_B \\ F_B \end{bmatrix} = A_{static} F_{dec} . \quad (2.9)$$

Where  $F_{dec}$  is the decomposed force vector defined as follow

$$F_{dec} = \begin{pmatrix} F_{h,1} \\ F_{v,1} \\ \dots \\ F_{h,n} \\ F_{v,n} \end{pmatrix}, \quad (2.10)$$

with  $F_{v,1} = \kappa_f \cos(\alpha_i)$  the vertical force produced by the i-th propeller and  $F_{h,1} = \kappa_f \sin(\alpha_i)$  the horizontal force produced by the i-th propeller. And the static matrix defined as

$$A_{static} = \begin{bmatrix} -\kappa_f L s(\beta_{arm,1}) c(\theta_{arm,1}) + c_1 \kappa_m s(\theta_{arm,1}) & +\kappa_f L s(\theta_{arm,1}) + c_1 \kappa_m c(\theta_{arm,1}) s(\beta_{arm,1}) & \dots & \dots \\ -\kappa_f L s(\beta_{arm,1}) s(\theta_{arm,1}) - c_1 \kappa_m c(\theta_{arm,1}) & -\kappa_f L c(\theta_{arm,1}) + c_1 \kappa_m s(\beta_{arm,1}) s(\theta_{arm,1}) & \dots & \dots \\ -L \kappa_f c(\beta_{arm,1}) & c_1 \kappa_m c(\beta_{arm,1}) & \dots & \dots \\ s(\theta_{arm,1}) \kappa_f & s(\beta_{arm,1}) c(\theta_{arm,1}) \kappa_f & \dots & \dots \\ -c(\theta_{arm,1}) \kappa_f & s(\beta_{arm,1}) s(\theta_{arm,1}) \kappa_f & \dots & \dots \\ 0 & c(\beta_{arm,1}) \kappa_f & \dots & \dots \end{bmatrix}$$

a  $6 \times 2n$  matrix that is invariant for a drone design. Using the Moore-Penrose pseudo inverse we can easily get the inverse kinematic as

$$F_{dec} = A_{static}^\dagger \begin{bmatrix} M_{des} \\ F_{des} \end{bmatrix}. \quad (2.11)$$

Which returns the decomposed force vector for a desired force and torque. Finding the tilting angles and propellers rotation speed required to attain this desired force and torque is then

$$\begin{cases} w_i^2 = \frac{1}{\kappa_f} \sqrt{F_{v,i}^2 + F_{h,i}^2} \\ \alpha_i = \text{atan2}(F_{h,i}, F_{v,i}) \end{cases}. \quad (2.12)$$

## 2.2 Optimization problem

The following section focuses on the optimization problem that the tool has to solve in order to obtain a MAV design that is optimal. The criteria that make this design optimal are also discussed.

### Problem statement

The optimization problem is stated as follow

$$\arg \max_x f(x) \quad \text{subject to} \quad \begin{cases} c(x) \leq 0 \\ ceq(x) = 0 \\ A \cdot x \leq 0 \\ Aeq \cdot x = 0 \\ lb \leq x \leq ub, \end{cases} \quad (2.13)$$

where  $f(x)$  is the cost function,  $x$  the argument vector,  $c(x)$  the non-linear inequality constraint vector,  $ceq(x)$  the non-linear equality constraint vector,  $A$  the linear inequality constraint matrix,  $Aeq$  the linear equality constraint matrix,  $lb$  the lower bound vector of the arguments ( $x$ ) and  $ub$  the upper bound vector.

Once the optimization problem solved, the output is the optimal argument vector  $x^*$  that maximizes the cost function  $f(x)$ . In our case the argument vector  $x$  is composed of the MAV's morphology parameters ( $\beta_{arm}$ ,  $\theta_{arm}$ ,  $L$ ,  $n$ ) and the cost functions are the subject of the next section.

### Cost Functions

As stated in Chapter 1, the aim of the project is to obtain a multi-rotor design that is omni-directional. Therefore, it is the heart of the problem to define meaningful cost functions for the optimization problem, which when solved will return parameters for an omni-directional drone. In this section, the few cost functions that capture the omni-directionality are described.

The first cost function consists in maximizing the minimal attainable force and the minimal attainable torque that the MAV can produce in any direction. The omni-directionality is defined as the drone capacity to accelerate instantaneously in every direction. In order to do that the MAV has to have high minimal attainable force and torque, hence this cost function. It turns out that this cost function is also computationally less demanding for the solver than the others. Indeed, when the multi-rotor MAV applies a force or torque in the direction parallel to one of its arms, the propeller on this arm is perfectly unable to produce any force or torque in this direction. This is due to the fact that no matter what the tilting angle for this propeller is, the thrust it produces is parallel to the arm directions (see Figure 2.2). Therefore, the minimal attainable forces and torques for the drone are in the directions towards which one of the propeller can't apply any thrust, i.e. the arm directions. So instead of optimizing the force and torque in a large number of directions, it is enough for this cost function to optimize the force and torque in  $n$  directions.

The second cost function consist of maximizing the minimal attainable force and the minimal attainable torque that the MAV can produce in any direction and minimizing the MAV's inertia. It is the same as the first cost function, but the last term is added in order to add a criterion on the controllability and thus have an easier drone to control and .

The next cost function is designed to maximize the volume of the reachable force and torque space. The force and torque spaces are two polyhedrons formed by the drone's attainable forces and torques in every direction (see Figure 2.4a and Figure 2.4b). The idea behind this cost function is to have the biggest task space for the drone and hence increase the MAV's ability to navigate in any orientation and to any position. This cost function is computationally heavy for the solver, because in order to have precise polyhedrons for the different spaces, the forces and torques have to be computed in at least 578 directions.

Another cost function that maximizes the force, the torque and the hover efficiency in all directions is developed. The aim of this cost function is to maximize the agility of the MAV for good disturbance rejection. Moreover, the term that maximizes the hover efficiency is designed to give the drone the ability to efficiently perform manipulations in any orientation. Solving the optimization problem for this cost function can also be computationally heavy depending on how many effective directions you choose to represent all directions.

The last cost function maximizes the force and the torque in one defined direction  $d$ . It is mostly designed to test the optimization tool as it is computationally light and, given specific directions, the optimal design is evident. For instance, if you maximize the force in the  $Z$  direction for a 4-rotor MAV, the expected optimal solution would be a traditional quad-copter. The presented cost functions use the multi-rotor model described in Section 2.1 to compute the different forces and torques in the different directions.

### Solver

To solve the problem in Equation (2.13), the tool uses the MATLAB<sup>®</sup> function fmincon, with different algorithms. The one showing the quickest convergence and

the best results being the sequential quadratic programming (sqp) algorithm.

## 2.3 Optimization tool

As explained above, an optimization tool has been developed to perform the design optimization of the drone and return information on the resulting design. In this section the tool is exposed and its working principle is explained.

### User Guide

To use the tool, the graphical user interface (GUI) represented in Figure 2.3 first has to be opened. Then, the parameters to optimize have to be selected. The choice is between optimizing just  $\beta_{arm}$  angles, or  $\beta_{arm}$  angles with other selected parameters (see Figure 2.3). Afterwards, the design parameters that are not selected for the optimization have to be specified. For instance, if the arm length is not to be optimized, the user has to specify an arm length. To solve the optimization the sqp algorithm needs an initial solution. Hence, an initial solution is expected from the user. Then the cost function has to be chosen from the list (see Figure 2.3). Finally, in order to obtain a result the user needs to push the “start optimization” button.

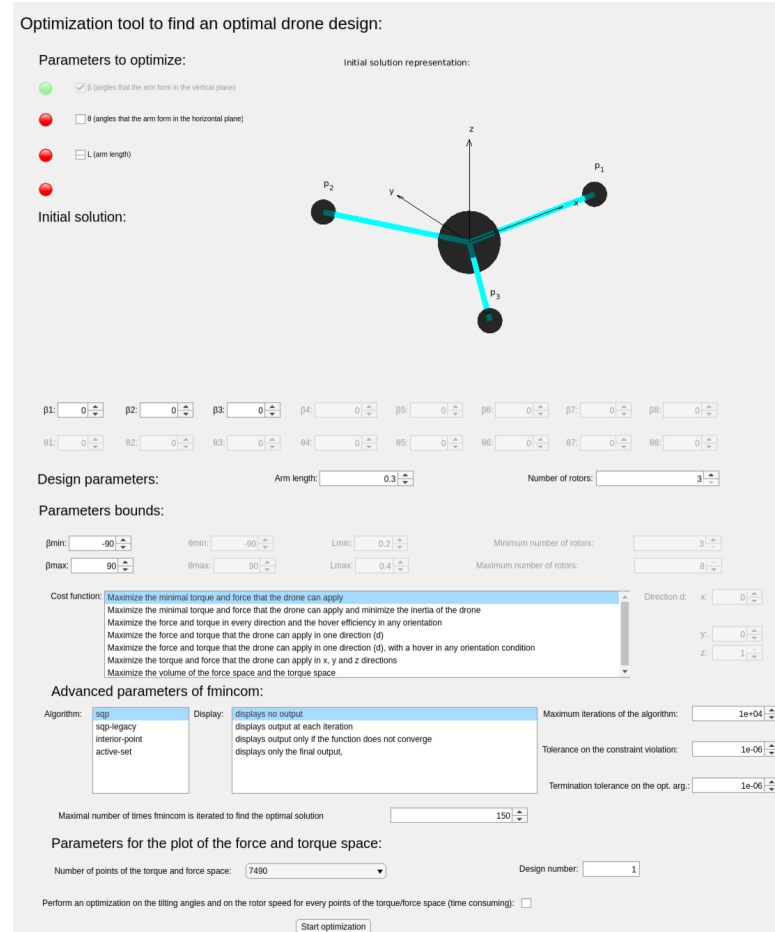


Figure 2.3: MAV morphology optimization tool GUI.

## Outcome

Apart from the optimal design parameters ( $\beta_{arm}$ ,  $\theta_{arm}$ ,  $L$  and  $n$ ), the optimization tool returns a MATLAB® plot containing the attainable force space, the attainable torque space, the hover efficiency in every orientation and a schematic of the MAV's design (see Figure 2.4). It is important to note that the force and torque space and the hover efficiency diagram are all represented in the drone's body frame. And thus, in the force and torque space diagrams, the dots that can be observed in Figure 2.4a represent the directions equally distributed around the MAV's body center. The distance between a point and the center of the body is proportional to the magnitude of the maximal force or torque that the drone can apply in this direction. The color of this point correspond to the efficiency of the force or torque in this direction, calculated as

$$F_{eff} = \frac{\|Force_{attainable \text{ in } direction}\|}{\|Thrust_{produced \text{ in total}}\|}, M_{eff} = \frac{\|Torque_{attainable \text{ in } direction}\|}{\|L \cdot Thrust_{produced \text{ in total}}\|}.$$

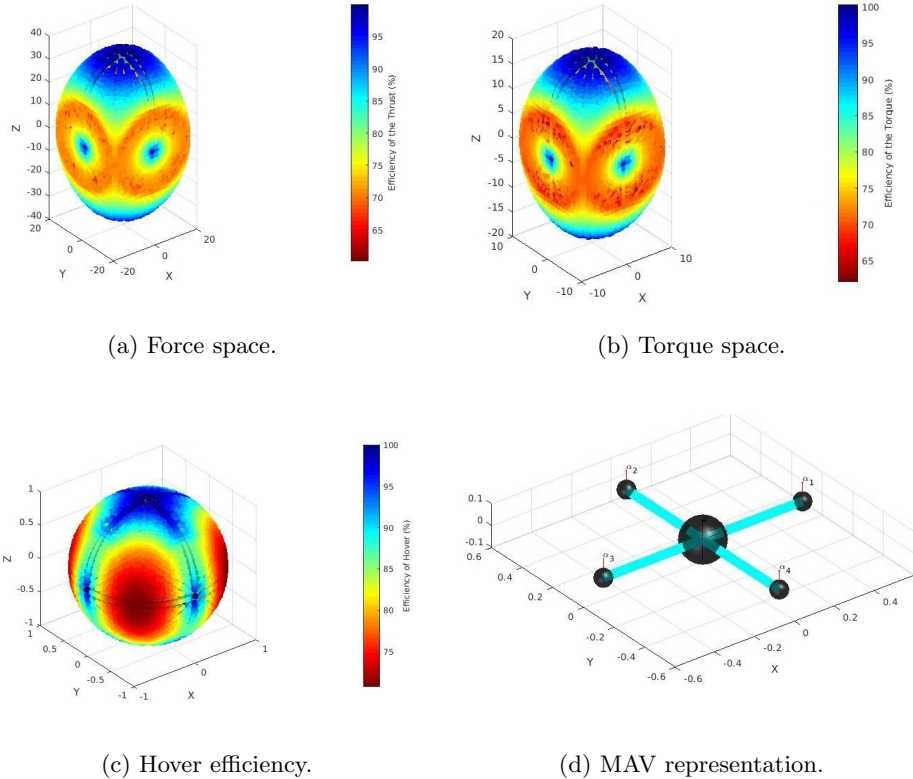


Figure 2.4: Example of the figures that the optimization tool outputs.

Along with the design parameters and the figure the optimization tool also provides information on the drone capabilities called metrics. These metrics are listed in Table 2.1.

Table 2.1: List of the metrics returned by the optimization tool.

Metrics:	Minimal	Maximal	Mean	MAD	Task space volume	Task space surface
Force:	[N]	[N]	[N]	[N]	[N <sup>3</sup> ]	[N <sup>2</sup> ]
Torque:	[Nm]	[Nm]	[Nm]	[Nm]	[N <sup>3</sup> m <sup>3</sup> ]	[N <sup>2</sup> m <sup>2</sup> ]
Hover efficiency:	[%]	[%]	[%]	[%]	-	-

### Limitations

Due to the non-linearity of the cost functions and the fact that the algorithms available in MATLAB® only guarantee convergence to local optima, the solution returned by the tool is strongly dependent on the chosen initial solution. Moreover, the more parameters one wants to optimize, the more the algorithms can be trapped in local optima.

## 2.4 Simulation Approach

As said above, a few of the optimal designs are tested in simulation on Gazebo®. In order to be simulated on Gazebo® a robot model, which is created in a Unified Robot Description Format<sup>4</sup> (URDF) file, is first launched on Gazebo®. In the mean time, a ROS node to control the robot's joints is launched and the simulation can start (see Figure 2.5). To simulate the chosen optimal MAV designs, they first have to be modeled in URDF files. Once it is done, the ROS node responsible for the control of the MAV, that is referred to as the control node, has to be built. The access to Voliro's control node was granted during the present work [5]. Therefore, to properly control the different design of MAV obtained, only a few changes were needed on Voliro's control node. First, the controller node had to be generalized for a n-rotor drone (opposed to a 6-rotor drone for Voliro). Then, the static allocation matrix (which is how Voliro transforms a desired angular and linear acceleration into desired motor speeds and rotor tilting angles) had to be generalized to a n-rotor MAV with an arbitrary arm orientation. Finally, because the arbitrary arm orientation can cause a center of mass (CoM) offset, an additional angular acceleration had to be added to the desired angular acceleration, in order to compensate for the CoM offset. This angular acceleration is calculated as follow

$$\dot{\omega}_{CoM} = -I_B^{-1}(R_{CoM} \times m\ddot{p}_{des}), \quad (2.14)$$

where  $R_{CoM}$  is the CoM position vector and  $\ddot{p}_{des}$  the desired linear acceleration. Once all these changes were made, the MAV model could be controlled in Gazebo® as illustrated in Figure 2.5).

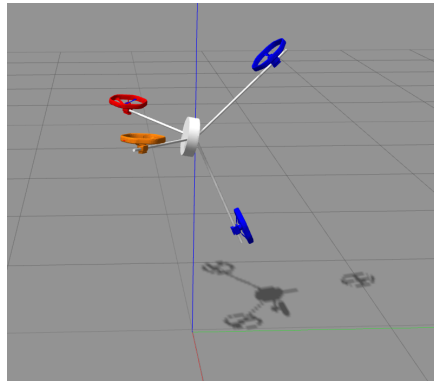


Figure 2.5: 4-rotor MAV design successfully launched and controlled in Gazebo®.

---

<sup>4</sup>Format based on XML used to represent robot models in ROS.

# Chapter 3

# Optimization Results

This chapter focuses on showing and analyzing the most interesting MAV designs produced by the optimization tool. First, a short digression on platonic solid is presented before analysing the results. The optimal designs with an even number of propellers, as well as the optimal designs with an odd number of propellers are shown. Finally, a comparison of the different optimal drone designs is then proposed.

## 3.1 Platonic Solids

Platonic solids are five regular and convex polyhedrons named in honor of the ancient Greek philosopher Plato [12]. The five platonic solids are:

- The tetrahedron composed of four faces and four vertices (see Figure 3.1a).
- The octahedron composed of eight faces and six vertices (see Figure 3.1b).
- The cube composed of six faces and eight vertices (see Figure 3.1c).
- The icosahedron composed of twenty faces and twelve vertices.
- The dodecahedron composed of twelve faces and twenty vertices.

An angle can be found in the first three platonic solids. This angle is found between the horizontal plane and the vertices of the polyhedron (see Figure 3.1). As explained below, this angle can also be found in some of the obtained results. Therefore, in order to ensure simplicity, in the rest of this thesis this angle will be referred to as the platonic solids' angle ( $\beta_{PS}$ ).

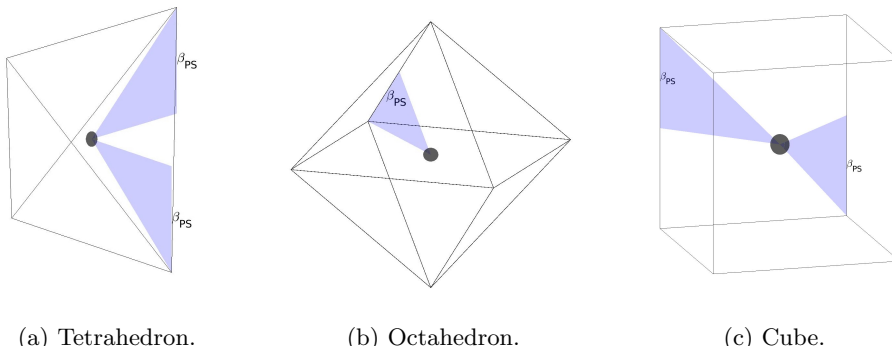


Figure 3.1: The angle  $\beta_{PS}$  in the first three platonic solids ( $\cos(\beta_{PS}) = \sqrt{\frac{2}{3}} \rightarrow \beta_{PS} \simeq 35.26^\circ$ ).

## 3.2 Even Designs

### 3.2.1 Quad-copter

The first MAV morphology presented is obtained when optimizing to find  $\beta_{arm}$  and  $\theta_{arm}$ , with  $n = 4$  and  $L = 0.5 [m]$  as fixed design parameters and  $\beta_{arm,0} = [0^\circ, 0^\circ, 0^\circ, 0^\circ]$  and  $\theta_{arm,0} = [0^\circ, 0^\circ, 0^\circ, 0^\circ]$  as initial solution. The cost function used to solve the optimization problem, is the one that maximizes the minimal attainable force and the minimal attainable torque that the MAV can produce in any direction while it minimizes the inertia of the drone. The result is depicted in Figure 3.2a and has the following features:

- $n = 4$
- $\beta_{arm} = [-32.42^\circ, -35.49^\circ, -35.44^\circ, -35.49^\circ]$
- $\theta_{arm} = [-0.99^\circ, -1.88^\circ, -2.26^\circ, -2.94^\circ]$
- $L = 0.5 [m]$

It is noticeable that the angles  $\theta_{arm}$  tend towards zero and that the angles  $\beta_{arm}$  tend towards the platonic solid angle  $\beta_{PS}$ . However, the design has not totally converged. This is probably due to the fact that the optimization tool has, as mentioned in Section 2.3, found a local optimum before reaching the global one. The global optimum seems to occur when the drone has the arms equally distributed in the horizontal plane ( $\theta_{arm} = 0$ ) and forming the platonic solid angle with the same horizontal plane ( $\beta_{arm} = \beta_{PS}$ ). Therefore, to verify that the solution with the  $\beta_{PS}$  is optimal, a second design is obtained when performing the same optimization as before but this time choosing  $\beta_{arm,0} = [35.26^\circ, -35.26^\circ, 35.26^\circ, -35.26^\circ]$  as initial solution. The result in Figure 3.2a is defined by:

- $n = 4$
- $\beta_{arm} = [35.26^\circ, -35.26^\circ, 35.26^\circ, -35.26^\circ]$
- $\theta_{arm} = [0^\circ, 0^\circ, 0^\circ, 0^\circ]$
- $L = 0.5 [m]$

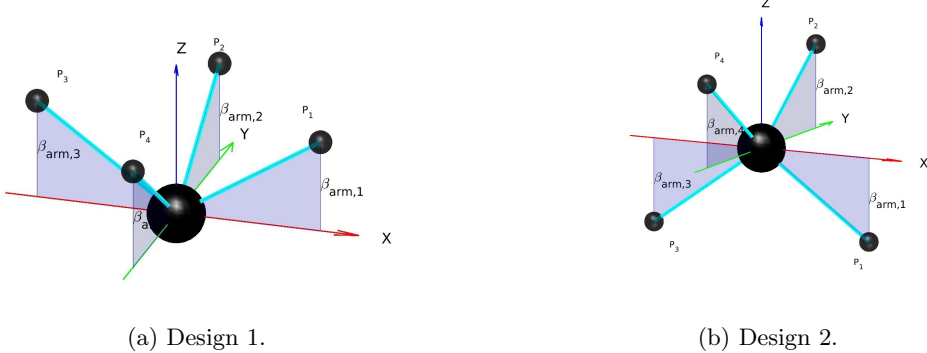


Figure 3.2: Representation of the designs obtained for the quad-copter.

After this second optimization, the second design is found to be identical to the initial solution. This means that the initially chosen design is optimal and is likely a global optimum since starting the optimization from different initial solutions makes the solver converges to this optimum. It is interesting to note that the four propellers of the second design form the four vertices of a tetrahedron (see Figure 3.3).

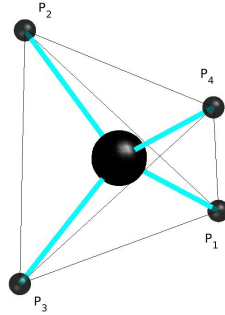


Figure 3.3: Design 2 within a tetrahedron.

It is important to understand that, for the tool, that the designs with all the arms oriented upwards (as design 1), or the designs with distributed arms (as design 2), are equivalent. When comparing Figure 3.4 with Figure 3.5 and when comparing the different metrics in Table 3.1, Table 3.2 and Table 3.3, despite slightly different arm angles' between the two designs, one can easily see that the two designs propose similar abilities. The main difference is the location of their center of mass which the tool does not consider. For instance, the second design's CoM coincides with the body origin, which renders the drone more balanced and thus easier to control.

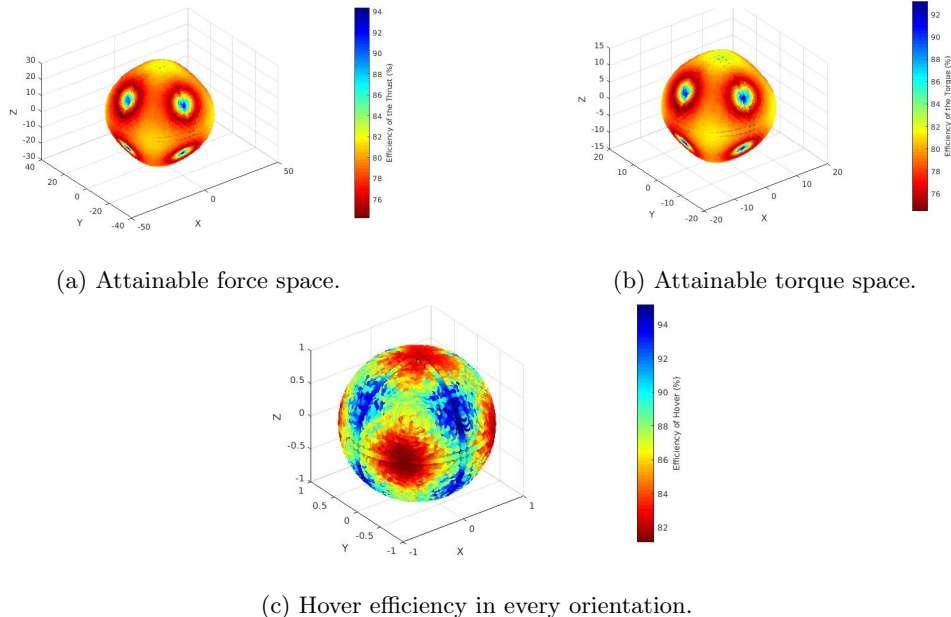


Figure 3.4: Visual representation of the abilities of design 1.

In the following tables, a comparison between the metrics of the optimal designs and the standard quad-copter is proposed. Due to the tilting ability of the rotors, the standard design is equally fully-actuated. Even though the force that the standard quad-copter design can apply in the  $Z$  direction is large, the forces that it can apply on its sides and in average are much more limited. We also notice that the optimal designs proposed by the tool are meeting the omni-directionality criteria

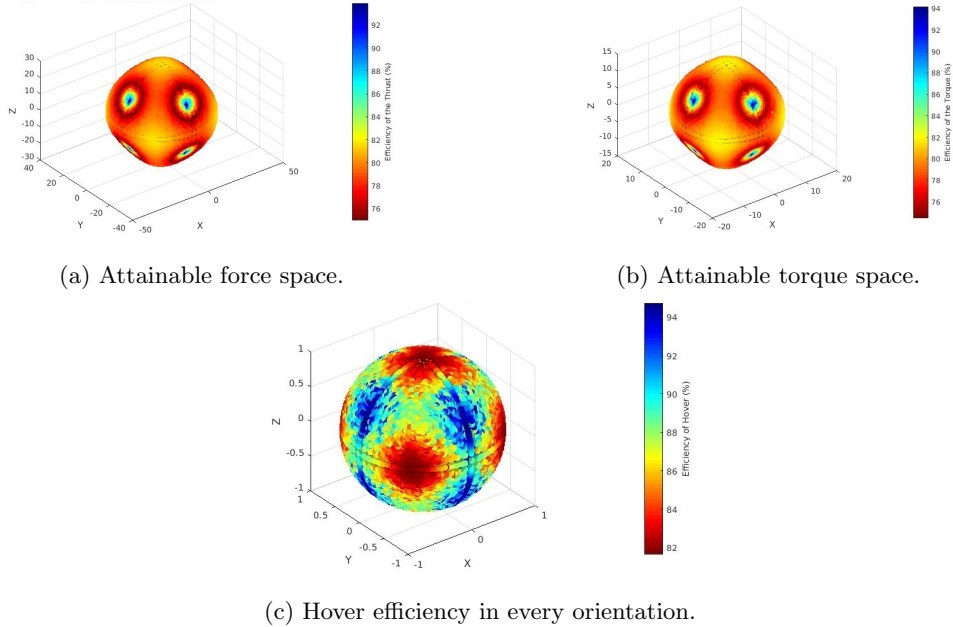


Figure 3.5: Visual representation of the abilities of design 2.

stated in Section 2.2. Indeed, compared to the standard design, the minimal forces and torques that the optimal designs can apply are high. Furthermore, the volumes of the attainable forces and torques are large and shaped like spheres, which makes the MAVs dynamical properties nearly invariant to their orientation. Therefore, they are omni-directional MAVs.

Table 3.1: Information on the designs' force space properties.

Design	$F_{min}$ [N]	$F_{max}$ [N]	$F_{mean}$ [N]	$MAD(F)$ [N]	Force space volume [ $N^3$ ]	Force space surface [ $N^2$ ]
1	23.19	28.56	26.87	0.86	81'683	9'345
2	23.23	28.37	26.87	0.86	81'710	9'326
Standard	17.37	34.74	24.43	3.43	65'673	8'865

Table 3.2: Information on the designs' torque space properties.

Design	$M_{min}$ [Nm]	$M_{max}$ [Nm]	$M_{mean}$ [Nm]	$MAD(M)$ [Nm]	Torque space volume [ $N^3 m^3$ ]	Torque space surface [ $N^2 m^2$ ]
1	11.62	14.32	13.47	0.43	10'298	2'355
2	11.65	14.23	13.47	0.43	10'300	2'348
Standard	8.7	17.42	12.25	1.72	8'284	2'219

Table 3.3: Information on the designs' hover efficiency space properties.

Design	$H_{eff,min}$ [%]	$H_{eff,max}$ [%]	$H_{eff,mean}$ [%]	$MAD(H_{eff})$ [%]
1	81.11	95.18	87.03	2.63
2	81.65	94.73	87.1	2.6
Standard	70.7	100	82.3	6.1

### 3.2.2 Hexa-copter

When optimizing to find  $\beta_{arm}$  and  $\theta_{arm}$ , with fixed design parameters  $n = 6$  and  $L = 0.5 [m]$  and as chosen cost function for the optimization problem the cost function that maximizes the volumes of the force and torque spaces, the tool returns a design defined by:

- $n = 6$
- $\beta_{arm} = [35.26^\circ, -35.26^\circ, 35.26^\circ, -35.26^\circ, 35.26^\circ, -35.26^\circ]$
- $\theta_{arm} = [0^\circ, 0^\circ, 0^\circ, 0^\circ, 0^\circ, 0^\circ]$
- $L = 0.5 [m]$

It is noteworthy that, even when using a different cost function to solve the omnidirectionality optimization problem, the arm angles  $\beta_{arm}$  converge to the platonic solid angle and that the propellers tend to from the platonic solid that matches their number. For instance, in this six propeller case, the optimal MAV design form is an octahedron (see Figure 3.7). In the rest of this section the optimal drone design depicted in Figure 3.6a is compared to the standard hexa-copter design, which is equivalent to Voliro presented in [5] (see Figure 3.6b).

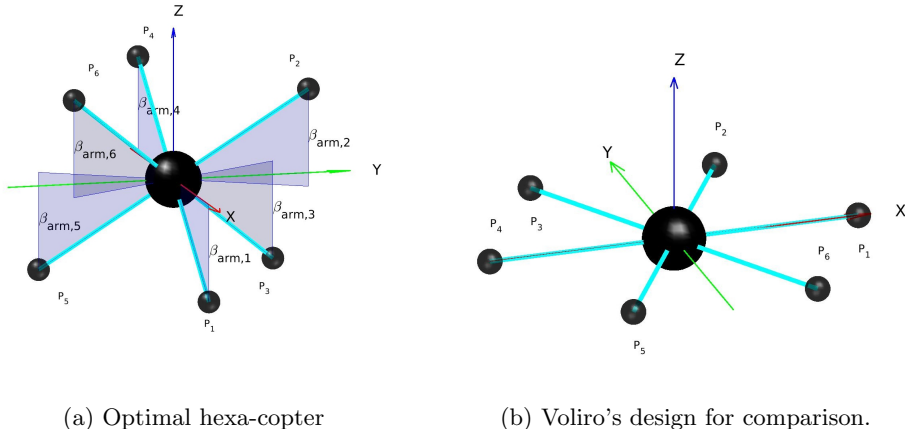


Figure 3.6: Representation of the design obtained for the hexa-copter.

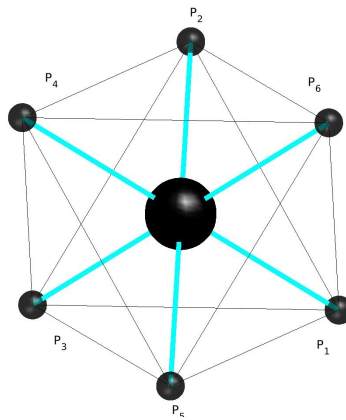


Figure 3.7: Optimal hexa-copter within an octahedron.

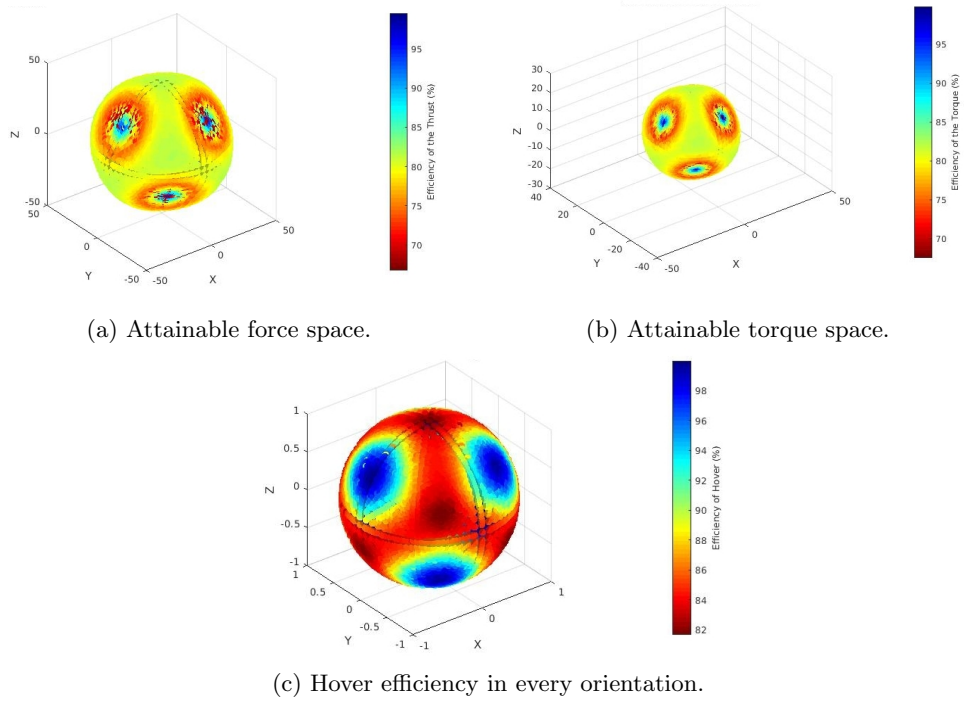


Figure 3.8: Visual representation of the abilities of the optimal hexa-copter.

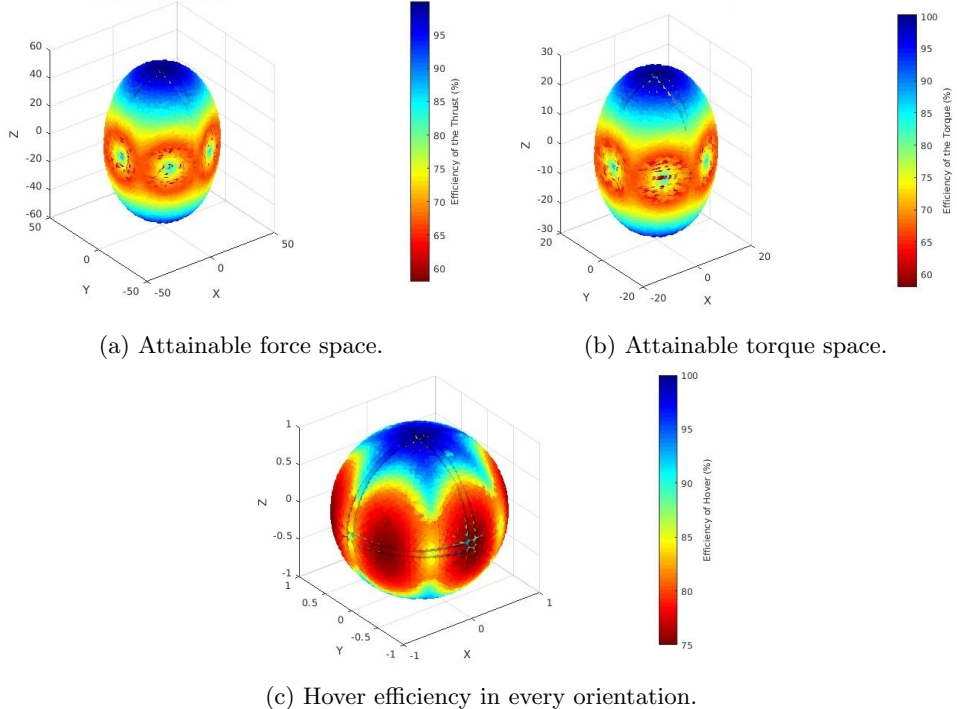


Figure 3.9: Visual representation of the abilities of Voliro.

When comparing the different spaces shown in Figure 3.8 and in Figure 3.9, the first noticeable characteristic is that the torque and force spaces of the optimal hexa-copter are much more spherical than Voliro's. Which makes the optimal hexa-copter's dynamical features more independent of its orientation. Then, one can without difficulty notice in Figure 3.9c that Voliro can only hover with a 100 % efficiency when oriented near the initial position or upside down. Whereas the newly obtained design can hover with a 100 % efficiency in at least six very different orientations (see Figure 3.8c). Furthermore, the hover efficiency is generally higher for the optimized design (see Table 3.6).

Table 3.4: Information on the designs' force space properties.

Design	$F_{min}$ [N]	$F_{max}$ [N]	$F_{mean}$ [N]	$MAD(F)$ [N]	Force space volume [ $N^3$ ]	Force space surface [ $N^2$ ]
Optimal hexa-copter	34.74	42.55	39.52	2.21	267'010	20'922
Voliro	26.6	52.11	37.77	4.33	244'293	20'170

Table 3.5: Information on the designs' torque space properties.

Design	$M_{min}$ [Nm]	$M_{max}$ [Nm]	$M_{mean}$ [Nm]	$MAD(M)$ [Nm]	Torque space volume [ $N^3m^3$ ]	Torque space surface [ $N^2m^2$ ]
Optimal hexa-copter	17.42	21.34	19.82	1.1	33'687	5'230
Voliro	15.09	26.13	18.94	2.17	30'788	5'121

Table 3.6: Information on the designs' hover efficiency space properties.

Design	$H_{eff,min}$ [%]	$H_{eff,max}$ [%]	$H_{eff,mean}$ [%]	$MAD(H_{eff})$ [%]
Optimal hexa-copter	81.65	100	88.92	4.43
Voliro	75	100	84.21	5.35

### 3.2.3 Octa-copter

The next result is obtained when the tool solves the optimization problem for an eight rotor MAV, with as a cost function, the one that maximizes the minimal attainable force and the minimal attainable torque that the MAV can produce in any direction and that minimizes the inertia of the drone. The result represented in Figure 3.10a is defined by:

- $n = 8$
- $\beta_{arm} = [35.26^\circ, -35.26^\circ, 35.26^\circ, -35.26^\circ, 35.26^\circ, -35.26^\circ, 35.26^\circ, -35.26^\circ]$
- $\theta_{arm} = [0^\circ, 0^\circ, 0^\circ, 0^\circ, 0^\circ, 0^\circ, 0^\circ, 0^\circ]$
- $L = 0.5$  [m]

The morphology converged once more to an even distribution of the arms in the horizontal plane and to  $\beta_{arm}$  equal to plus or minus  $\beta_{PS}$ . Out of curiosity, the obtained result is compared to the Omnicopter presented in [4]. However, for the sake of a meaningful comparison, it is assumed that the Omnicopter can dynamically tilt its rotors around their axes (see Figure 3.10b). The Omnicopter's design parameters are:

- $n = 8$
- $\beta_{arm} = [-35.26^\circ, -35.26^\circ, -35.26^\circ, -35.26^\circ, 35.26^\circ, 35.26^\circ, 35.26^\circ, 35.26^\circ]$
- $\theta_{arm} = [0^\circ, 45^\circ, 90^\circ, 135^\circ, 180^\circ, -135^\circ, -90^\circ, -45^\circ]$
- $L = 0.5$  [m]

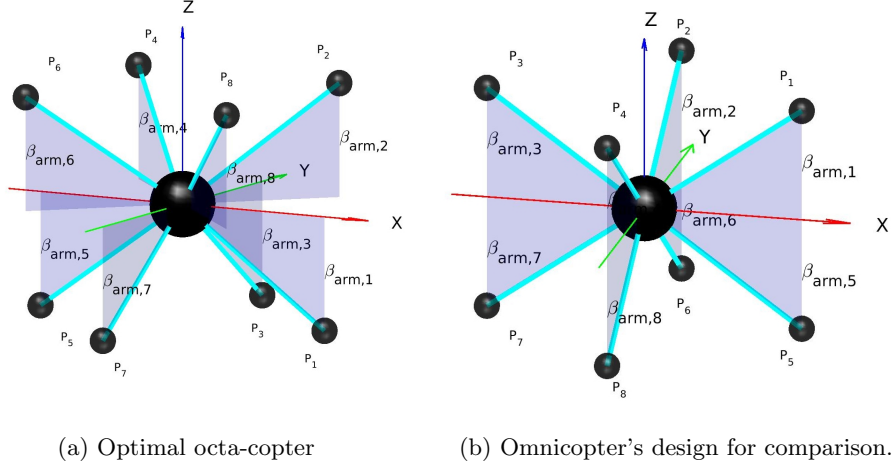


Figure 3.10: Representation of the designs obtained for the octa-copter.

It is interesting to note that this time the design returned by the tool does not form a platonic solid with its propellers, but the Omnicopter does (see Figure 3.11).

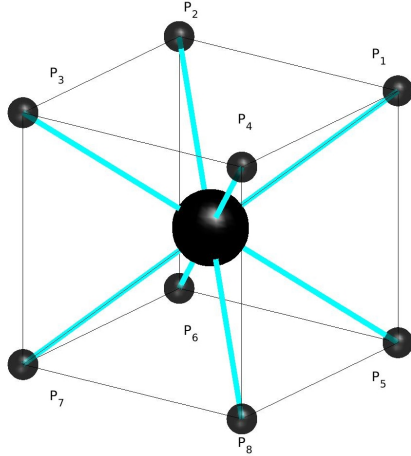


Figure 3.11: Omnicopter in a cube.

When comparing the two designs' features represented in Figure 3.13 and Figure 3.12 and detailed in Table 3.7, Table 3.8 and Table 3.9, one notices that the two design are quite similar. Nevertheless, the arms of the optimal octa-copter are more evenly distributed, this leads to a slightly bigger torque and force space volume and an average hover efficiency which is better for the optimal octa-copter.

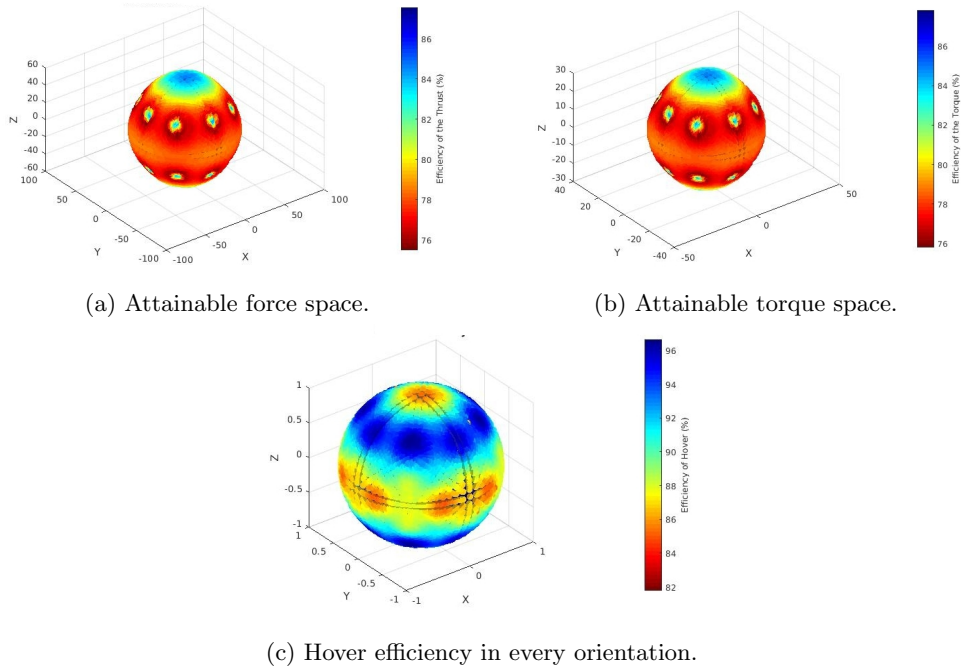


Figure 3.12: Visual representation of the abilities of the optimal octa-copter.

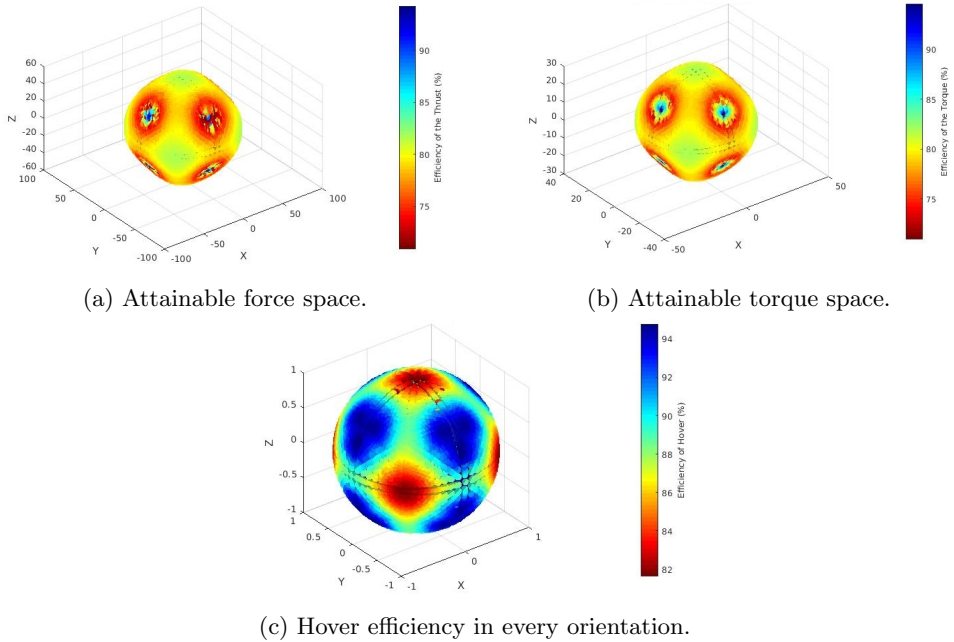


Figure 3.13: Visual representation of the abilities of the Omnicopter.

Table 3.7: Information on the designs' force space properties.

Design	$F_{min}$ [N]	$F_{max}$ [N]	$F_{mean}$ [N]	$MAD(F)$ [N]	Force space volume [ $N^3$ ]	Force space surface [ $N^2$ ]
Optimal octa-copter	44.7	58.78	53.95	0.94	669'339	37'625
Omnicopter	46.46	56.73	53.75	1.72	653'736	37'263

Table 3.8: Information on the designs' torque space properties.

Design	$M_{min}$ [Nm]	$M_{max}$ [Nm]	$M_{mean}$ [Nm]	$MAD(M)$ [Nm]	Torque space volume [ $N^3m^3$ ]	Torque space surface [ $N^2m^2$ ]
Optimal octa-copter	22.4	29.48	27	0.47	84'417	9'463
Omnicopter	23.3	28.45	26.95	0.86	82'446	9'374

Table 3.9: Information on the designs' hover efficiency space properties.

Design	$H_{eff,min}$ [%]	$H_{eff,max}$ [%]	$H_{eff,mean}$ [%]	$MAD(H_{eff})$ [%]
Optimal octa-copter	81.78	96.65	91.42	2.7
Omnicopter	81.64	94.77	89.36	2.82

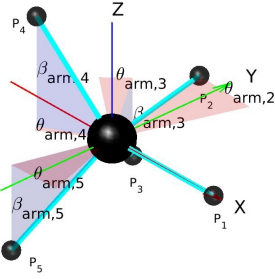
### 3.3 Odd Designs

#### 3.3.1 Penta-copter

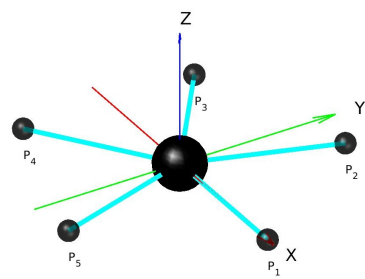
The next MAV design presented is interesting, indeed the optimization tool converged to an optimal solution, which is odd. This result was obtained when solving the morphology optimization problem for a five-rotor drone, with as a cost function, the one that maximizes the force, the torque and the hover efficiency in all directions. For this optimization,  $\beta_{arm,1}$ ,  $\beta_{arm,2}$  and  $\theta_{arm,1}$  are forced to be zero, in order for the tool to have less parameters to optimize and thus to be more precise. The morphology obtained is represented in Figure 3.14a and its parameters are:

- $n = 5$
- $\beta_{arm} = [0^\circ, 0^\circ, 36.89^\circ, -58.46^\circ, 41.45^\circ]$
- $\theta_{arm} = [0^\circ, 30.3^\circ, -16.13^\circ, -5.46^\circ, -33.37^\circ]$
- $L = 0.5$  [m]

In order to understand why the optimization tool found this unique design, with its seemingly random arm placement, a comparison with the standard tilting-rotor penta-copter is proposed. First, a visual comparison of the two designs is found in Figure 3.14.



(a) Optimal penta-copter.



(b) Penta-copter standard.

Figure 3.14: Schematic of different possible designs for a Penta-copter.

Even though the arm angles seem very peculiar in this optimal penta-copter, the propellers appear to be quite evenly disposed around the MAV. Hence, when looking at Figure 3.15a and Figure 3.15b the force and torque spaces of the optimal penta-copter are close to a sphere's shape, and when looking at Figure 3.15c the hover efficiency displayed by this design seems outstanding. And when examining the values showed in Table 3.10, Table 3.11 and Table 3.12 the first impressions are confirmed, despite rather low minimal attainable force and torque, this optimal design shows a very good average hover efficiency.

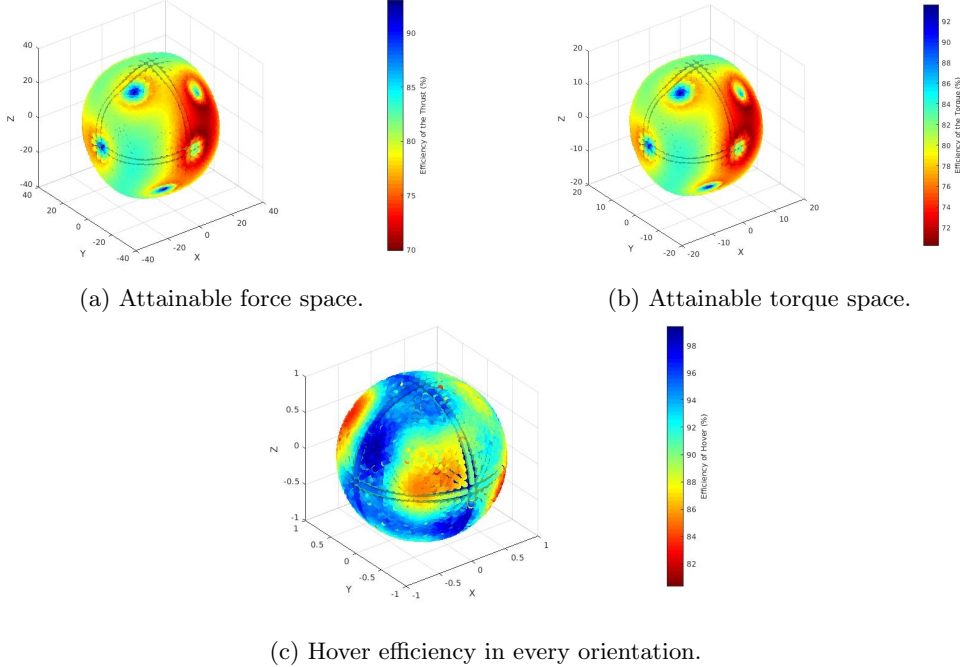


Figure 3.15: Visual representation of the abilities of the optimal penta-copter.

Table 3.10: Information on the designs' force space properties.

Design	$F_{min}$ [N]	$F_{max}$ [N]	$F_{mean}$ [N]	$MAD(F)$ [N]	Force space volume [ $N^3$ ]	Force space surface [ $N^2$ ]
Optimal	26.03	36.22	33.69	1.39	160'333	14'626
Standard	26.24	43.42	31.93	3.25	146'006	14'137

Table 3.11: Information on the designs' torque space properties.

Design	$M_{min}$ [Nm]	$M_{max}$ [Nm]	$M_{mean}$ [Nm]	$MAD(M)$ [Nm]	Torque space volume [ $N^3 m^3$ ]	Torque space surface [ $N^2 m^2$ ]
Optimal	12.85	18.2	16.93	0.7	20'358	3'741
Standard	10.9	21.8	16	1.63	18'409	3'580

Table 3.12: Information on the designs' hover efficiency space properties.

Design	$H_{eff,min}$ [%]	$H_{eff,max}$ [%]	$H_{eff,mean}$ [%]	$MAD(H_{eff})$ [%]
Optimal	80.33	99.4	90.96	3
Standard	77.25	100	84.38	5.2

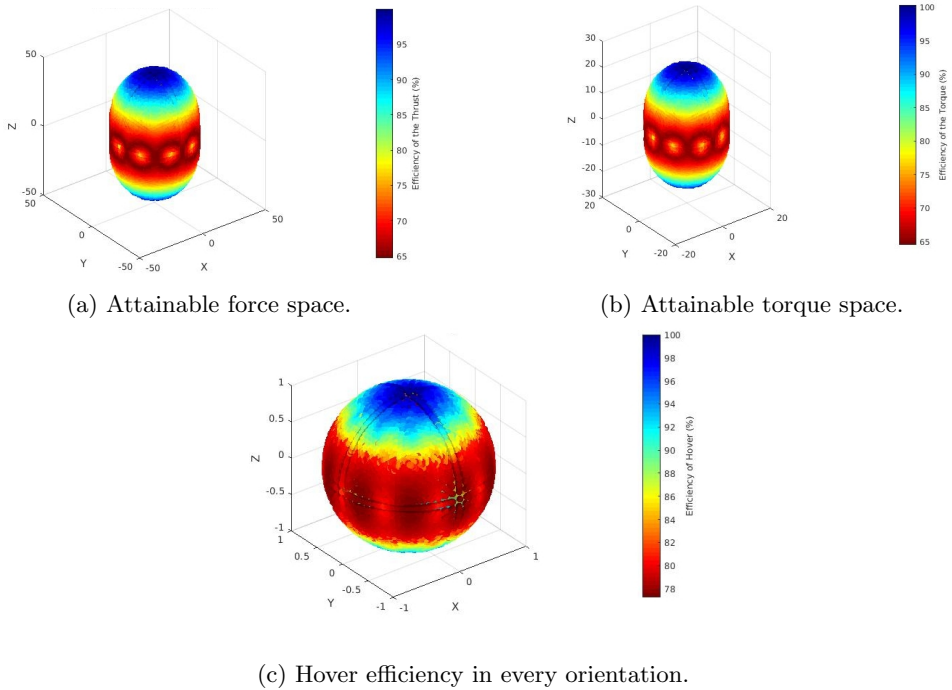


Figure 3.16: Visual representation of the abilities of the standard penta-copter.

### 3.3.2 Hepta-copter

The last design of this section is a very interesting design. Once more optimizing the arm angles in order to obtain the maximal minimum attainable force and torque, the following result was obtained from the tool. The design is represented in Figure 3.17a and is defined by:

- $n = 7$
- $\beta_{arm} = [35.26^\circ, 35.26^\circ, 35.26^\circ, 35.26^\circ, 35.26^\circ, 35.26^\circ, 35.26^\circ]$
- $\theta_{arm} = [0^\circ, 0^\circ, 0^\circ, 0^\circ, 0^\circ, 0^\circ, 0^\circ]$
- $L = 0.5 \text{ [m]}$

The  $\beta_{arm}$  fully converged to the  $\beta_{PS}$  angle, but in contrast with the optimal designs with an even number of propeller, this optimal design has all its arms oriented downwards. As explained in Section 3.2.1, the designs with the arms oriented of  $\beta_{PS}$  downwards and the design with the arms alternatively oriented of  $\beta_{PS}$  upwards and downwards are equivalent (for an even number of propeller). The only difference is a change in the CoM position. However, for the designs with an odd number of propellers, the arms can not be alternatively oriented with  $\beta_{PS}$  upwards and downwards. This would lead to two consecutive arms tilted downwards or upwards and thus an unbalanced design. However, despite the control inconvenience due to the CoM offset, this hepta-copter optimal design is very interesting, because the arms oriented downwards would leave place on the top of the MAV for a manipulator with a decent task space. Furthermore, when analyzing this design's hover efficiency space in Figure 3.17d one can notice that, except when the drone is in its initial position as in Figure 3.17a), the drone displays a very good hover efficiency. It would thus be a perfect design for aerial manipulation.

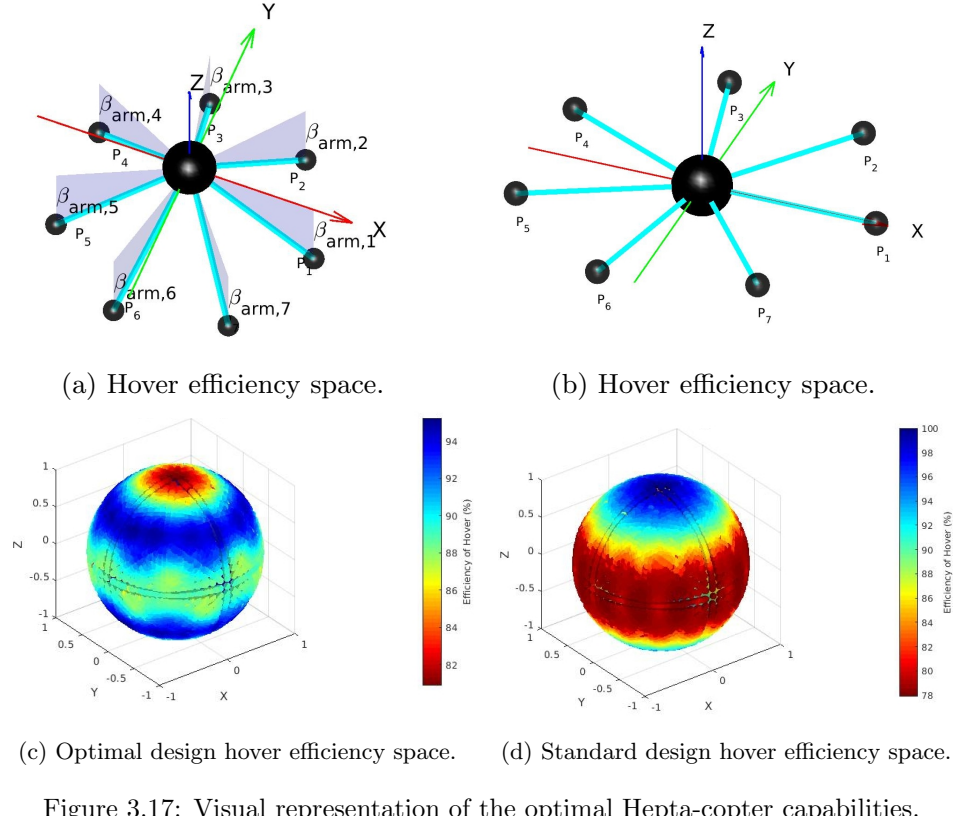


Figure 3.17: Visual representation of the optimal Hepta-copter capabilities.

### 3.4 Comparison of Different Designs

From the results discussed above, it is possible to draw a general conclusion on the omni-directional MAVs with tilting rotors. Indeed, the design of a n-rotor MAV is optimally omni-directional when the arms of the drone are evenly distributed on the horizontal plane, and when they all form an angle of  $|\beta| = 35.26^\circ$  with the same horizontal plane. Furthermore, the  $\beta$  angles have to be alternatively oriented upwards and downwards if  $n$  is even, or all oriented downwards if  $n$  is odd. The designs arising from this "law" for  $n = 3$  to  $n = 8$  are represented in Figure 3.18 And the information on their abilities is shown in Table 3.13, Table 3.14 and Table 3.15. From these figures, depending on their needs, one can choose one of those designs. For instance, if the aim is to do aerial manipulation with decent payloads, the hepta-copter seems to be ideal. In contrast the hexa-copter, which would not be the ideal design to mount a manipulator, would perform well when filming or taking pictures in any position at any orientation, for example in bridge inspection or film making.

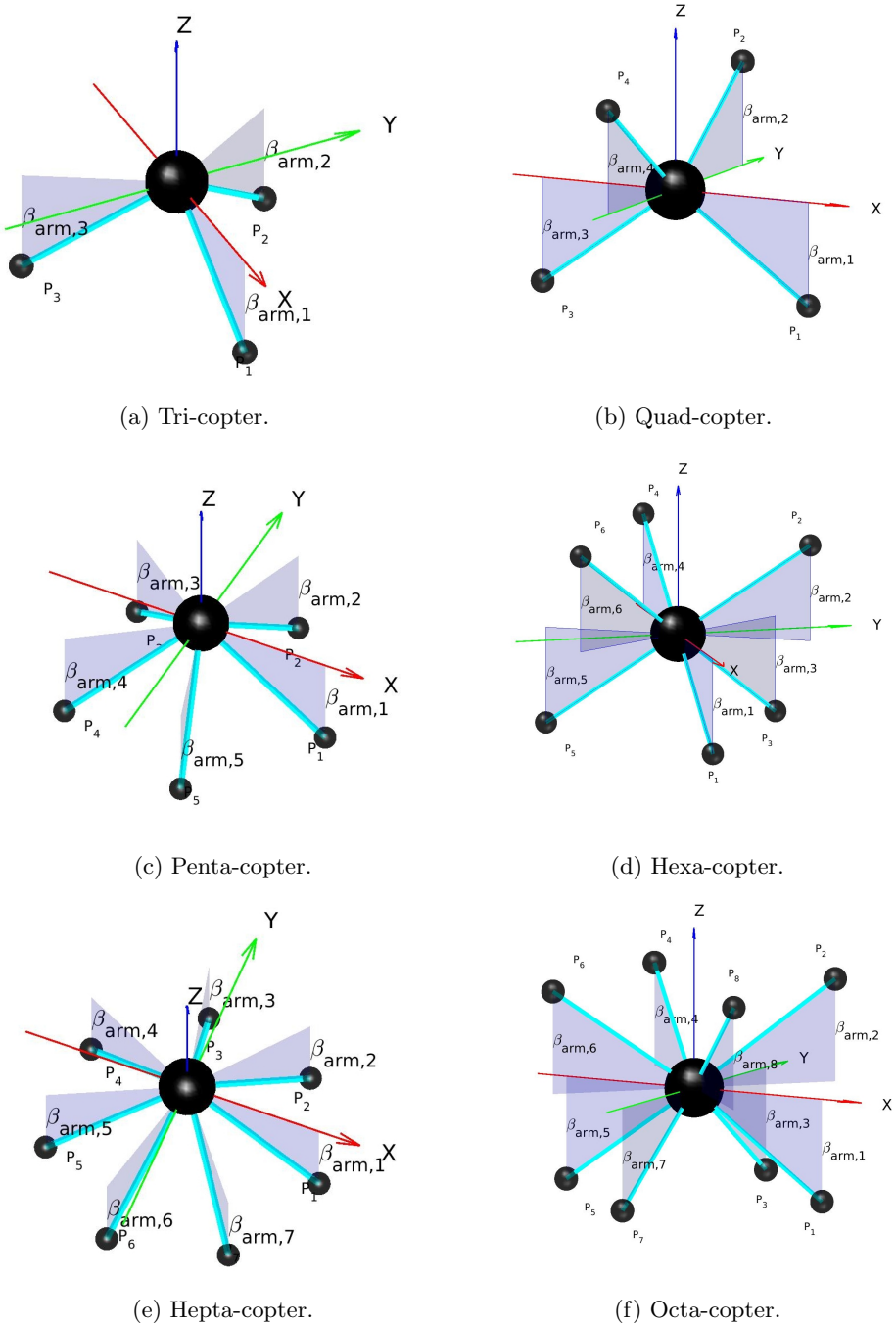


Figure 3.18: Representation of all the optimal designs.

Table 3.13: Comparison between all the different optimal designs' force space properties.

Design	$F_{min}$ [N]	$F_{max}$ [N]	$F_{mean}$ [N]	$MAD(F)$ [N]	Force space volume [ $N^3$ ]	Force space surface [ $N^2$ ]
Tri-copter	17.37	21.27	19.73	1.1	33'217	5'313
Quad-copter	23.23	28.37	26.87	0.86	81'710	9'326
Penta-copter	28.95	35.46	29.39	0.46	107'463	11'130
Hexa-copter	34.74	42.55	39.52	2.21	267'010	20'922
Hepta-copter	39.96	49.44	47.18	0.96	447'344	28'929
Octa-copter	44.7	58.78	53.95	0.94	669'339	37'625

Table 3.14: Comparison between all the different optimal designs' torque space properties.

Design	$M_{min}$ [Nm]	$M_{max}$ [Nm]	$M_{mean}$ [Nm]	$MAD(M)$ [Nm]	Torque space volume [ $N^3m^3$ ]	Torque space surface [ $N^2m^2$ ]
Tri-copter	8.7	10.67	9.87	0.56	4'158	1'379
Quad-copter	11.65	14.23	13.47	0.43	10'300	2'348
Penta-copter	14.52	17.78	14.74	0.23	13'555	2'800
Hexa-copter	17.42	21.34	19.82	1.1	33'687	5'230
Hepta-copter	20.04	24.8	23.66	0.48	56'403	7'304
Octa-copter	22.4	29.48	27	0.47	84'417	9'463

Table 3.15: Comparison between all the different optimal designs' hover efficiency space properties.

Design	$H_{eff,min}$ [%]	$H_{eff,max}$ [%]	$H_{eff,mean}$ [%]	$MAD(H_{eff})$ [%]
Tri-copter	81.65	99	87.22	4.42
Quads-copter	81.65	94.73	87.1	2.6
Penta-copter	81.65	91.43	85.35	1.49
Hexa-copter	81.65	100	88.92	4.43
Hepta-copter	80.88	95.23	91.1	2.4
Octa-copter	81.78	96.65	91.42	2.7



# Chapter 4

## Simulation Results

All the designs presented in Section 3.4 are tested in simulation. As explained in Chapter 2, they are simulated in Gazebo® and controlled by the means of a ROS node. These simulations are performed to evaluate the feasibility and the controllability of the theoretical optimal designs obtained in Chapter 3. As a first result it is important to state that all the MAVs tested in simulation were controlled properly and could maneuver well. Hence, all the optimal designs presented in Section 3.4 from the tri-copter to the octa-copter are feasible. The simulations also allow for comparison between different MAVs' dynamical abilities.

In this section the most interesting simulation results obtained are presented. First, a flight test performed by the tri-copter depicted in Figure 3.18a is presented, then a comparison between the hexa-copter shown in Figure 3.18d and the Voliro from [5] is proposed. Finally, a manipulation example with the hepta-copter presented in Section 3.3.2 is shown.

### 4.1 Tri-copter

The tri-copter with tilting rotor is a very interesting case because it is holonomic, which means that it has exactly six degrees of freedom (DoF) and evolves in a three dimensional space. Therefore, it should theoretically be able to produce forces and torques in any direction. To verify that a test flight is performed where the MAV hovers at one meter above the ground and changes its orientation up to a pitch angle  $\theta$  equal to  $90^\circ$ . The results of this test can be observed in Figure 4.1 and this observation of a quarter pitch flip illustrates the fact that the tri-copter is indeed able to hover in any orientation.

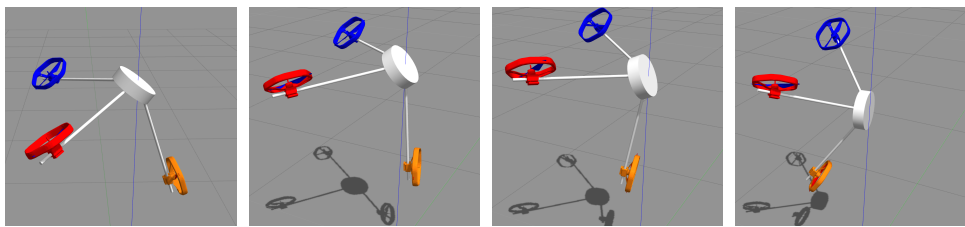


Figure 4.1: Simulation of the tri-copter in Gazebo.

## 4.2 Hexa-copter

The aim of this section is to compare the abilities of Voliro shown in Figure 4.2a with those of the optimal hexa-copter shown in Figure 4.2b. In order to do so, two maneuvers were performed with each of the MAVs in Gazebo®.

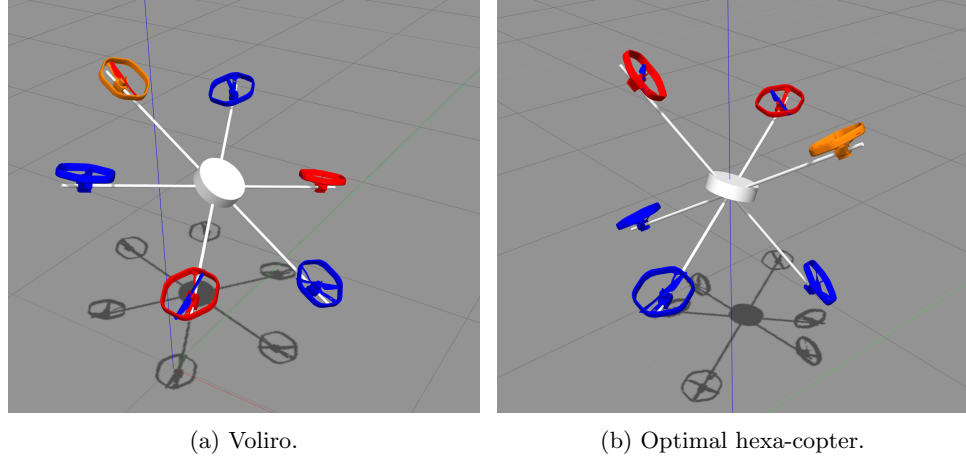


Figure 4.2: Representation of two six-rotor MAV models spawned in Gazebo®.

The first maneuver was a position tracking exercise, where the drones followed a trajectory describing two rounds of a circle, one meter above the ground at a speed of  $0.63 \frac{m}{s}$ . The graphs shown in Figure 4.3 and Figure 4.4 are the trajectory tracking plots. The graphs in Figure 4.5 and Figure 4.6 illustrate the orientation errors produced by the MAVs while following this circular trajectory. The second maneuver was an orientation tracking exercise, where the drones took off, hovered one meter above the ground for a few seconds, and then performed a full pitch flip, to finally land. The graphs shown in Figure 4.7 and Figure 4.8 are the trajectory tracking plots of this maneuver. The graphs in Figure 4.9 and Figure 4.10 illustrate the orientation tracking plot of the pitch flip.

First, when comparing Figure 4.3 with Figure 4.4 it is noteworthy that the optimal hexa-copter tracks the position with less delay. Then, when comparing Figure 4.5 with Figure 4.6, one can notice that even though the orientation error is very small for both designs, Voliro's is jittering more and slightly larger. When looking at the orientation tracking graphs in Figure 4.9 and in Figure 4.10, it is interesting to see that both designs performed well in this exercise. However, in Figure 4.9 there are two small overshoots in the orientation tracking. This is due to the fact that the controller uses the static allocation described in Section 2.1 to compute the desired tilting angles and speed for the rotors. This static matrix becomes singular in certain orientations and it leads to the loss of full-actuation in those orientations. This happens among others when one arm is oriented vertically. One can notice that this orientational instability happened only once for the hexa-copter's pitch flip (see Figure 4.10). This is because the hexa-copter only has one arm oriented vertically when performing the pitch flip. It is a consequence of the even distribution of the propellers in the space around the body that makes this MAV's dynamical properties really balanced.

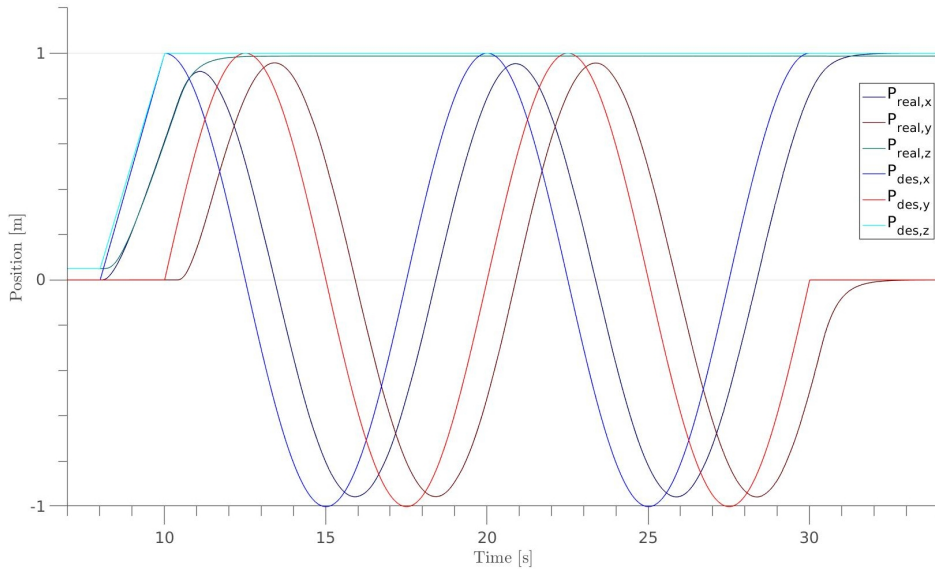


Figure 4.3: Trajectory tracking of a one meter circle performed by Voliro.

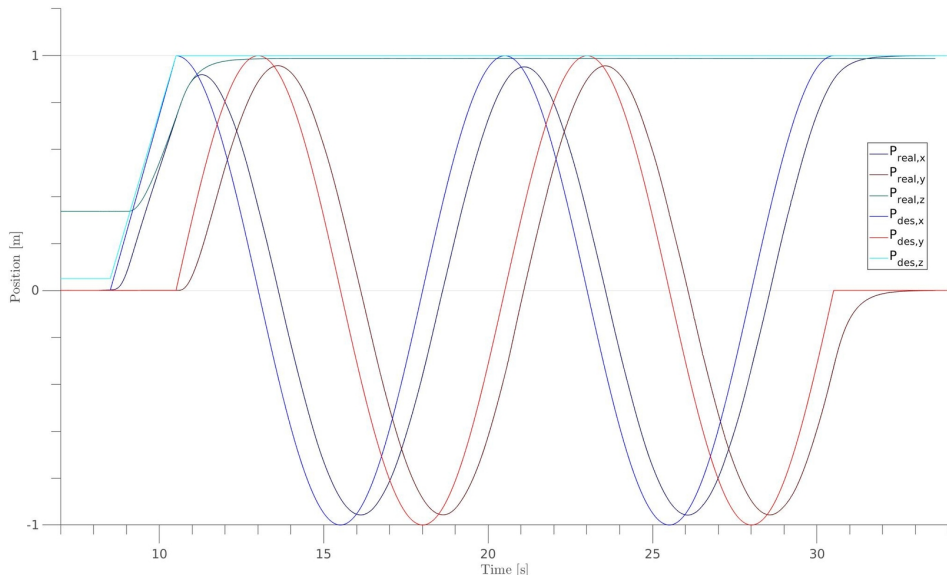


Figure 4.4: Trajectory tracking of a one meter circle performed by the optimal hexa-copter.

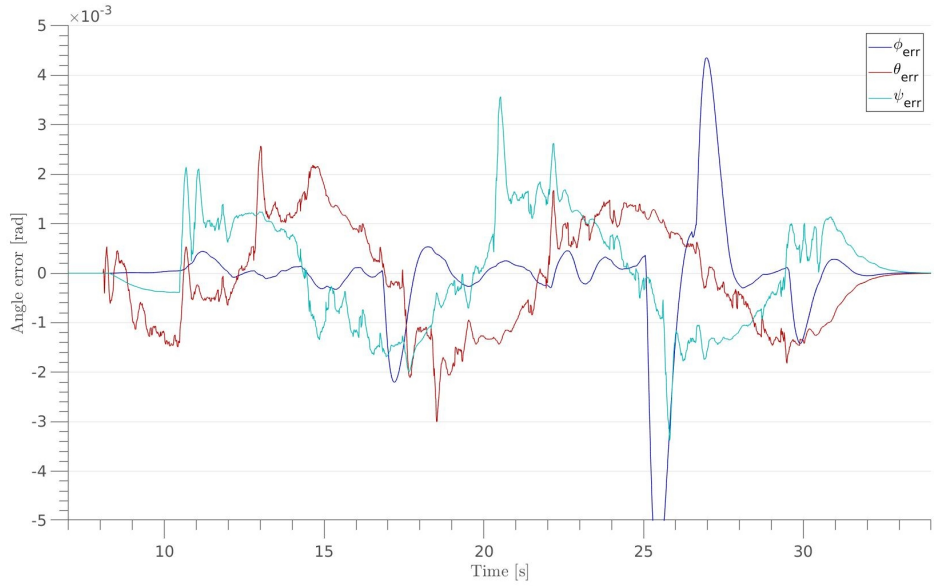


Figure 4.5: Pitch, roll and yaw angle errors when Voliro tracks a one meter circle.

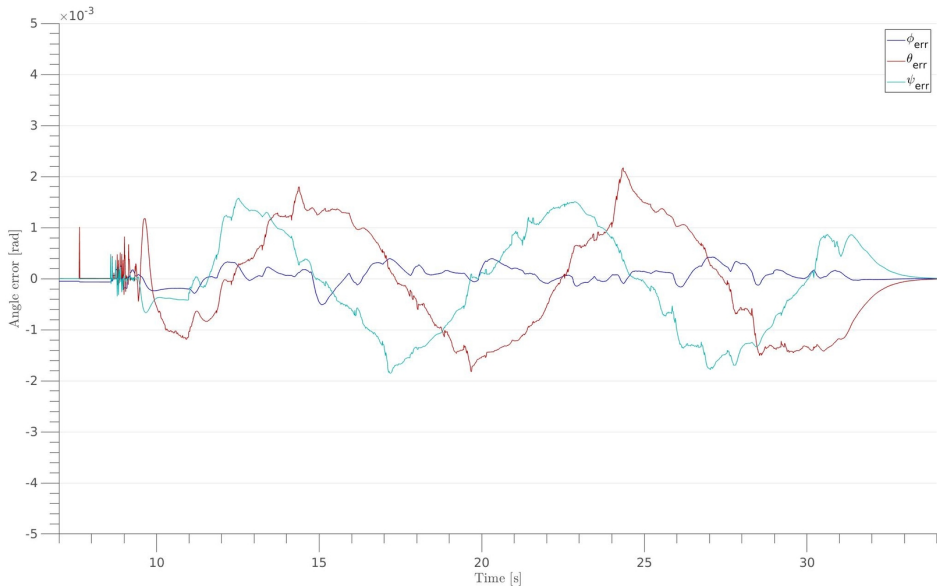


Figure 4.6: Pitch, roll and yaw angle errors when the optimal hexa-copter tracks a one meter circle.

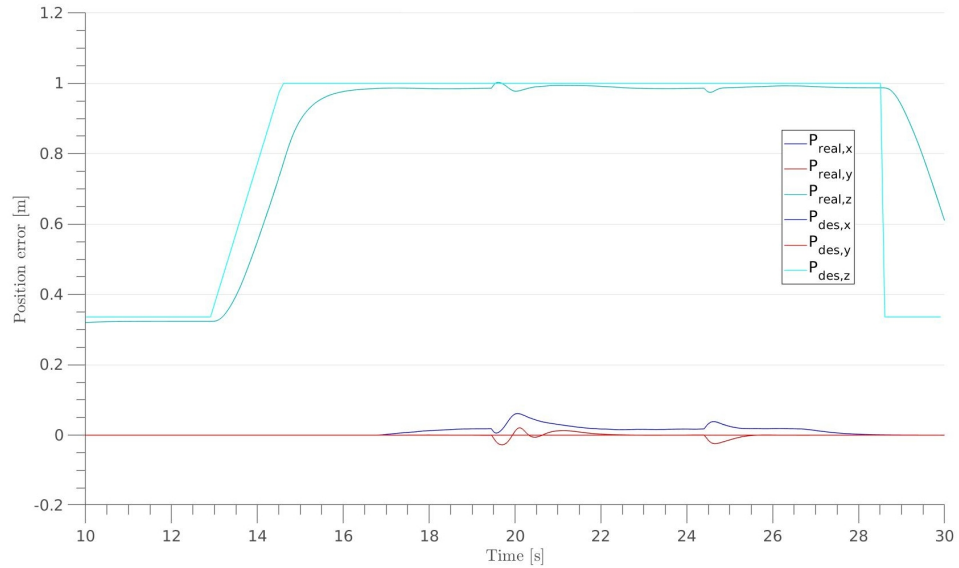


Figure 4.7: Trajectory tracking for Voliro performing a full pitch flip.

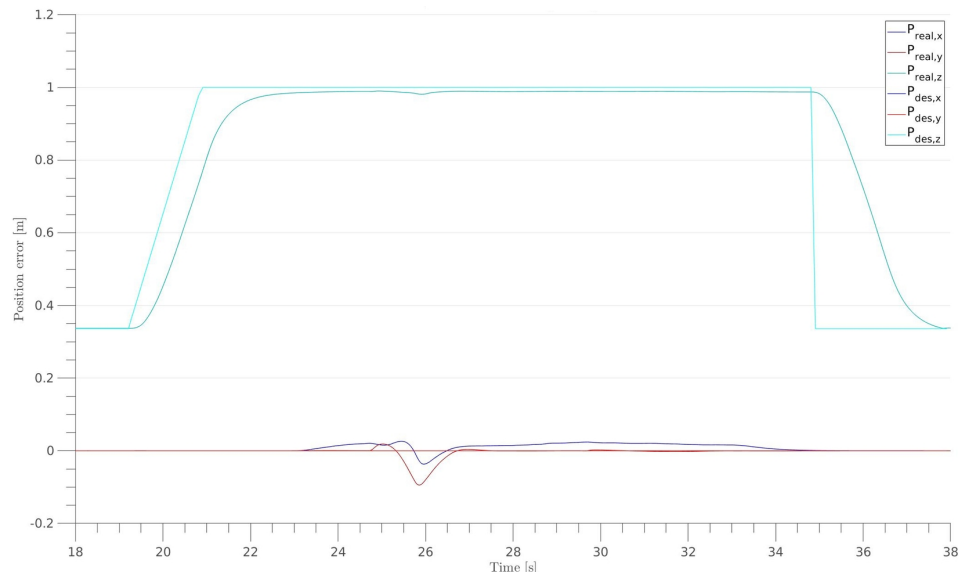


Figure 4.8: Trajectory tracking for the optimal hexa-copter performing a full pitch flip.

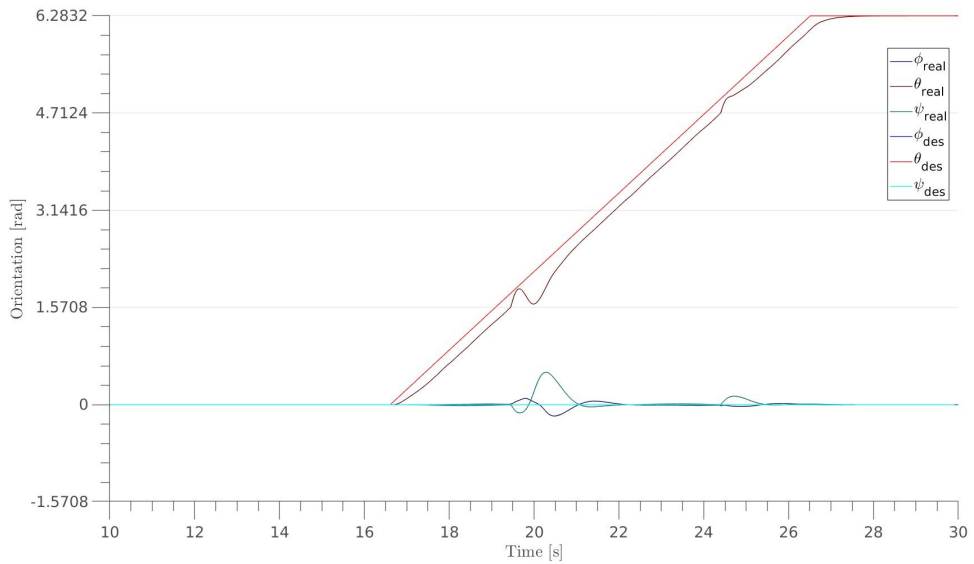


Figure 4.9: Pitch, roll and yaw angle tracking for Voliro performing a full pitch flip.

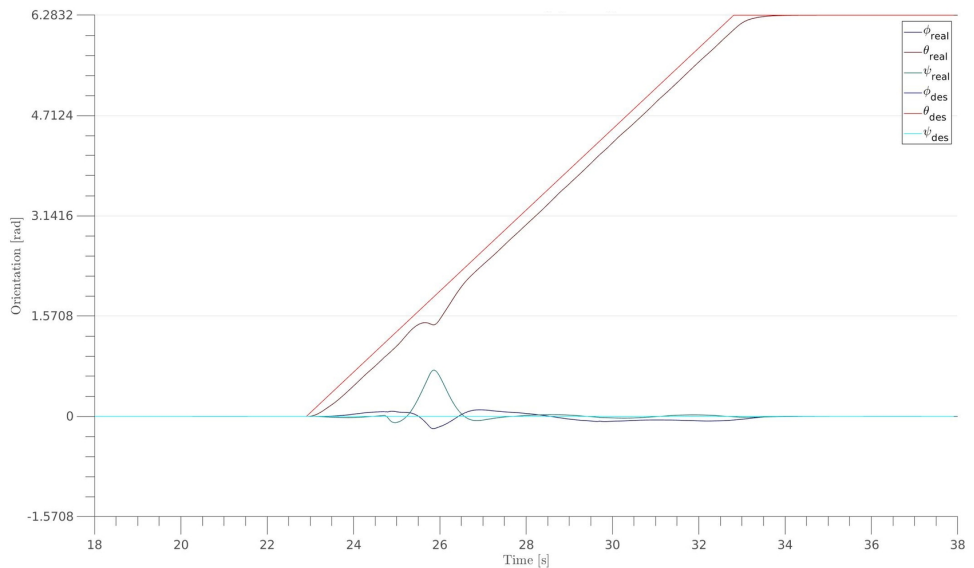


Figure 4.10: Pitch, roll and yaw angle tracking for the optimal hexa-copter performing a full pitch flip.

### 4.3 Hepta-copter

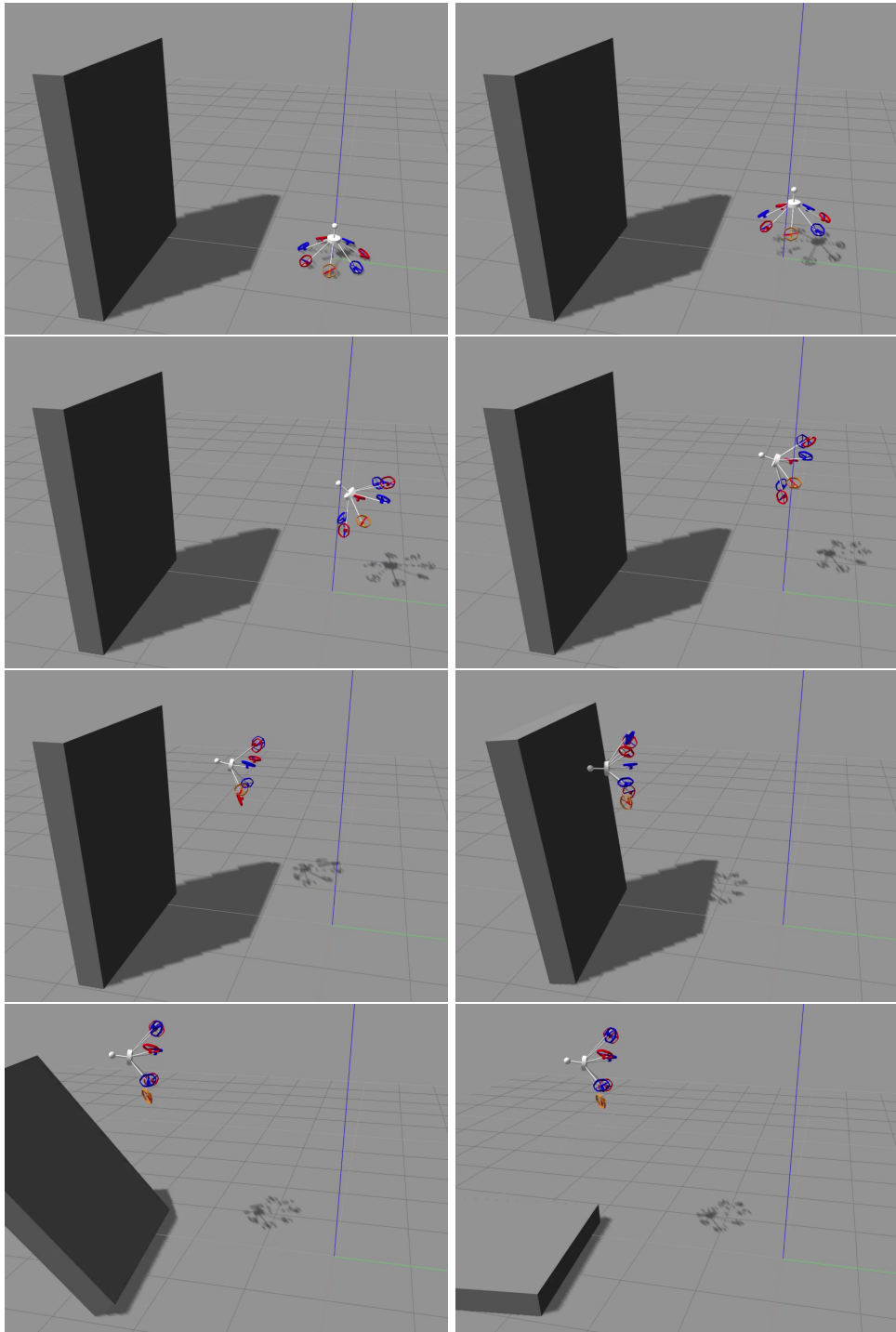


Figure 4.11: Slideshow of an interaction between the optimal hepta-copter and a wall.

The slide show above illustrate a manipulation task performed with the optimal

hepta-copter design obtained in Section 3.3.2. The MAV is used to demolish a wall (see Figure 4.11) . Although it is a very light wall of 1 [ $kg$ ], which falls easily on the ground this test represents quite well the omni-directionality and the manipulation capabilities of the hepta-copter.

# **Chapter 5**

## **Conclusion**

In this master's thesis, the problem of optimizing the morphology of several omni-directional rotary-wing micro aerial platforms was investigated. A general MAV model was first studied for the purpose of characterizing the drones' morphology. Different optimization problems were developed based on different criteria defining the omni-directionality. A tool was elaborated in the MATLAB® computing environment to solve these different optimization problems. A number of optimal multi-rotor MAVs were acquired by this tool and analyzed, thus allowing the formulation of a general "law" on the optimal omni-directional MAV morphology for the drones concerned in this work. While testing the different vehicles' design in a simulation environment proved their feasibility and their controllability, the lack of experimentation on a real prototype for the verification of different effects is still outstanding.

Future work therefore includes, the development of prototypes to do tests in real life to characterize the disturbance rejection abilities of the designs, and to characterize the airflow interactions between the propellers. These are among effects not yet accounted for in the present approach. Furthermore, such prototypes would allow for tests of the interaction between the real world and the presente optimal designs.



# Bibliography

- [1] M. Silvagni, A. Tonoli, E. Zenerino, and M. Chiaberge, “Multipurpose UAV for search and rescue operations in mountain avalanche events,” *Geomatics, Natural Hazards and Risk*, vol. 8, no. 1, pp. 18–33, Jan. 2017.
- [2] DJI Mavic Pro & Mavic Pro Platinum – Every Creative Moment – DJI. <https://www.dji.com/mavic>. Accessed: 2018-09-03.
- [3] Aura. <https://aura-drone.com/us/>. Accessed: 2010-09-30.
- [4] D. Brescianini and R. D’Andrea, “Design, modeling and control of an omnidirectional aerial vehicle,” in *2016 IEEE International Conference on Robotics and Automation (ICRA)*, May 2016, pp. 3261–3266.
- [5] M. Kamel, S. Verling, O. Elkhatib, C. Sprecher, P. Wulkop, Z. Taylor, R. Siegwart, and I. Gilitschenski, “Voliro: An Omnidirectional Hexacopter With Tilttable Rotors,” *arXiv:1801.04581 [cs]*, Jan. 2018, arXiv: 1801.04581.
- [6] A. Nikou, G. C. Gavridis, and K. J. Kyriakopoulos, “Mechanical design, modelling and control of a novel aerial manipulator,” in *2015 IEEE International Conference on Robotics and Automation (ICRA)*, May 2015, pp. 4698–4703.
- [7] S. Rajappa, M. Ryll, H. H. Bülthoff, and A. Franchi, “Modeling, control and design optimization for a fully-actuated hexarotor aerial vehicle with tilted propellers,” in *2015 IEEE International Conference on Robotics and Automation (ICRA)*, May 2015, pp. 4006–4013.
- [8] “MATLAB,” <https://en.wikipedia.org/w/index.php?title=MATLAB&oldid=852828655>, Jul. 2018, (Online: accessed August 30, 2018).
- [9] “Gazebo,” <http://wiki.ros.org/ROS/Tutorials>, (Online: accessed September 3, 2018).
- [10] “ROS/Tutorials - ROS Wiki,” <http://wiki.ros.org/ROS/Tutorials>, (Online: accessed August 12, 2018).
- [11] M. Ryll, H. H. Bülthoff, and P. R. Giordano, “Modeling and control of a quadrotor UAV with tilting propellers,” in *2012 IEEE International Conference on Robotics and Automation*, May 2012, pp. 4606–4613.
- [12] “Solide de Platon,” [https://fr.wikipedia.org/w/index.php?title=Solide\\_de\\_Platon&oldid=150277971](https://fr.wikipedia.org/w/index.php?title=Solide_de_Platon&oldid=150277971), Jul. 2018, (Online: accessed September 7, 2018).



# Acknowledgements

I would like to thank Prof. Dr. Roland Siegwart for kindly accepting me in his laboratory and allowing me to be a part of this interesting project.  
I would also like to thank my supervisors Karen Bodie and Zachary Taylor for their valuable advice, their help and their availability.

